

## RESEARCH OUTPUTS / RÉSULTATS DE RECHERCHE

### **Simplified quantum chemistry methods to evaluate non-linear optical properties of large systems**

Löffelsender, Sarah; Beaujean, Pierre; de Wergifosse, Marc

*Published in:*

Wiley Interdisciplinary Reviews: Computational Molecular Science

*DOI:*

[10.1002/wcms.1695](https://doi.org/10.1002/wcms.1695)

*Publication date:*

2024

*Document Version*

Publisher's PDF, also known as Version of record

[Link to publication](#)

*Citation for pulished version (HARVARD):*

Löffelsender, S, Beaujean, P & de Wergifosse, M 2024, 'Simplified quantum chemistry methods to evaluate non-linear optical properties of large systems', *Wiley Interdisciplinary Reviews: Computational Molecular Science*, vol. 14, no. 1, e1695. <https://doi.org/10.1002/wcms.1695>

#### **General rights**

Copyright and moral rights for the publications made accessible in the public portal are retained by the authors and/or other copyright owners and it is a condition of accessing publications that users recognise and abide by the legal requirements associated with these rights.

- Users may download and print one copy of any publication from the public portal for the purpose of private study or research.
- You may not further distribute the material or use it for any profit-making activity or commercial gain
- You may freely distribute the URL identifying the publication in the public portal ?

#### **Take down policy**

If you believe that this document breaches copyright please contact us providing details, and we will remove access to the work immediately and investigate your claim.

## ADVANCED REVIEW

# Simplified quantum chemistry methods to evaluate non-linear optical properties of large systems

Sarah Löffelsender<sup>1</sup>  | Pierre Beaujean<sup>2</sup>  | Marc de Wergifosse<sup>3</sup> 

<sup>1</sup>Mulliken Center for Theoretical Chemistry, Clausius Institute of Physical and Theoretical Chemistry, University of Bonn, Bonn, Germany

<sup>2</sup>Laboratory of Theoretical Chemistry, Unit of Theoretical and Structural Physical Chemistry, Namur Institute of Structured Matter, University of Namur, Namur, Belgium

<sup>3</sup>Theoretical Chemistry Group, Molecular Chemistry, Materials and Catalysis Division (MOST), Institute of Condensed Matter and Nanosciences, Université Catholique de Louvain, Louvain-la-Neuve, Belgium

**Correspondence**

Marc de Wergifosse, TCG, MOST, IMCN, UCLouvain, Place Louis Pasteur 1, bte L4.01.02, B-1348 Louvain-la-Neuve, Belgium.  
Email: [marc.dewergifosse@uclouvain.be](mailto:marc.dewergifosse@uclouvain.be)

**Funding information**

Horizon 2020 Framework Programme (H2020) EuroCC project

**Edited by:** Anna Krylov, Associate Editor and Peter R. Schreiner, Editor-in-Chief

**Abstract**

This review presents the theoretical background concerning simplified quantum chemistry (sQC) methods to compute non-linear optical (NLO) properties and their applications to large systems. To evaluate any NLO responses such as hyperpolarizabilities or two-photon absorption (2PA), one should evidently perform first a ground state calculation and compute its response. Because of this, methods used to compute ground states of large systems are outlined, especially the xTB (extended tight-binding) scheme. An overview on approaches to compute excited state and response properties is given, emphasizing the simplified time-dependent density functional theory (sTD-DFT). The formalism of the eXact integral sTD-DFT (XsTD-DFT) method is also introduced. For the first hyperpolarizability, 2PA, excited state absorption, and second hyperpolarizability, a brief historical review is given on early-stage semi-empirical method applications to systems that were considered large at the time. Then, we showcase recent applications with sQC methods, especially the sTD-DFT scheme to large challenging systems such as fluorescent proteins or fluorescent organic nanoparticles as well as dynamic structural effects on flexible tryptophan-rich peptides and gramicidin A. Thanks to the sTD-DFT-xTB scheme, all-atom quantum chemistry methodologies are now possible for the computation of the first hyperpolarizability and 2PA of systems up to 5000 atoms. This review concludes by summing-up current and future method developments in the sQC framework as well as forthcoming applications on large systems.

This article is categorized under:

Electronic Structure Theory > Ab Initio Electronic Structure Methods  
Structure and Mechanism > Molecular Structures

Electronic Structure Theory > Density Functional Theory

Electronic Structure Theory > Semiempirical Electronic Structure Methods

**KEYWORDS**

excited state absorption, first hyperpolarizability, large systems, non-linear optical properties, simplified quantum chemistry, sTD-DFT, two-photon absorption

## 1 | INTRODUCTION

In her doctoral thesis,<sup>1</sup> Maria Gertrude Göppert-Mayer predicted in 1931 the existence of the two-photon absorption (2PA) as a non-linear optical (NLO) property of molecules (see Figure 1). Thirty years later, following the discovery of laser,<sup>2</sup> 2PA was observed for the first time by Kaiser and Garrett.<sup>3</sup> The same year, Franken et al.<sup>4</sup> proved the existence of the second harmonic generation (SHG). Shortly after, Terhune et al.<sup>5</sup> observed the third harmonic generation (THG). Thanks to high-intensity laser beams with well-defined properties, the experimental techniques to measure and characterize NLO properties were developed rapidly after, introducing electric-field induced SHG (EFISHG), hyper-Rayleigh scattering (HRS), Z-scan, fluorescence lifetime imaging microscopy (FLIM), and others.<sup>6</sup> Since then, properties of matter can be probed using NLO phenomena.<sup>7,8</sup> The design of new materials with enhanced NLO properties provided a wealth of new applications, including in data storages,<sup>9</sup> photonic devices, telecommunication,<sup>10</sup> biological imaging techniques,<sup>11–13</sup> and others.<sup>14</sup> Designing new materials with the desired enhanced NLO property remains experimentally challenging without any theoretical background to understand the underlying physical chemistry of the phenomenon. Thus, quantum mechanical (QM) calculations can play a noteworthy contribution into the design of new materials if and only if methods are available to treat such systems in reasonable amounts of time while keeping a decent accuracy. Unfortunately, such theoretical techniques did not emerge as fast as experimental approaches did, due to the relative complexity of the equations involved providing in praxis time- and memory-intensive calculations. Traditional ab initio methods such as time-dependent Hartree–Fock (TD-HF),<sup>15</sup> time-dependent density functional theory (TD-DFT),<sup>16</sup> response function (RF),<sup>17</sup> equation-of-motion (EOM)<sup>18</sup> coupled cluster (CC), or multireference perturbation theory (MRPT)<sup>19</sup> can now provide accurate results, but still at very high computational cost, jeopardizing their applications to large systems.

In the beginning of computer-based quantum chemistry (QC) response property calculations, it was only possible to calculate very small systems (<20 atoms) with ab initio methods. Then, semi-empirical methods (i.e., simplified versions of QM schemes) were developed, generally involving integral approximations and parameterizations against reference data.<sup>20</sup> 30 years ago, semi-empirical approaches were very important allowing to extract and test structure–property relationships and to study diversities of structures<sup>20,21</sup> that would have not been possible otherwise. However, already at the time, experiments were focusing on (very) large systems, which were out of the range of these methods because of computational requirements.

Nowadays, due to the evolution of modern computers, ab initio approaches can be routinely applied to evaluate NLO properties for systems containing up to 50 (post-HF methods) to 200 (HF and DFT) atoms. Still, ultra-large systems such as proteins, nanoparticles or surfaces are out of the range. To overcome this, modern simplified QC methods (sQC) provide an alternative route to study such compounds. Current sQC methods do not involve necessarily the use of a semi-empirical ground state but applied reasonable approximations to response equations like with the simplified

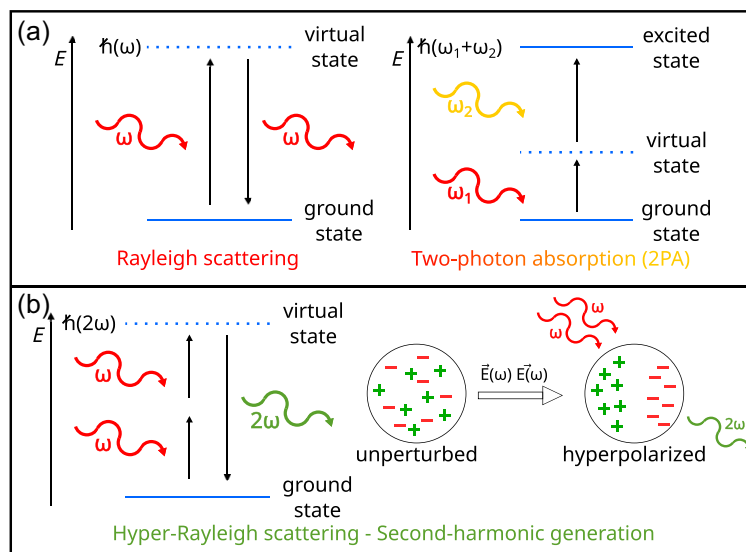


**FIGURE 1** Schematic overview of Rayleigh and Hyper-Rayleigh scattering as well as two-photon absorption.

time-dependent density functional theory (sTD-DFT).<sup>22</sup> Over the past decade, sQC methods were used to evaluate NLO response properties of increasingly large systems up to 5000 atoms such as the 2PA of explicitly solvated molecules,<sup>23</sup> excited state absorption of the photoactive yellow protein (PYP),<sup>24</sup> the first hyperpolarizability ( $\beta$ ) of functionalized surfaces,<sup>25</sup> metal complexes doped polymers,<sup>26</sup> fluorescent proteins (FPs),<sup>27</sup> and fluorescent organic nanoparticles (FONs).<sup>28</sup> Additionally, the availability of simplified methods allowed to explore dynamic structural effects on NLO response properties, for example, the 2PA of chromophores in proteins,<sup>29</sup> second-order NLO properties of tryptophan-rich oligomers,<sup>30</sup> and carbon-based nanomaterials with defects.<sup>31,32</sup> In such cases, simplified methods provided an excellent balance between accuracy and computational resources.

A recent perspective article on the evaluation of excited states and response properties using simplified QC methods by one of us<sup>22</sup> showed that the relevance of today's semi-empirical methods for the evaluation of NLO responses can be divided in two cases: (i) calculations on large systems (>500 atoms), where time and/or memory required per ab initio calculations prevent its routine use, and (ii) high-throughput/screening applications. In Section 2, the theory behind different sQC approaches is provided, especially for the sTD-DFT method. The eXact integral sTD-DFT (XsTD-DFT) method is introduced for the first time. Then, applications for the evaluation of the NLO properties of large systems are discussed in Section 3 while conclusions, future challenges, and outlooks are addressed in Section 4.

## 2 | THEORY

For a given geometry, the QC evaluation of any NLO property starts with (i) a ground state calculation followed by (ii) the computation of the property of interest. This section is divided in three parts. First, we briefly address the different approaches to obtain the ground state using the HF method and its semi-empirical counterparts (Section 2.1) as well as the density functional theory, density functional based tight binding, and extended tight-binding (xTB) methods (Section 2.2). Second, an overview of the different methods to compute molecular NLO properties especially with the sTD-DFT method is given in Section 2.3.

### 2.1 | The HF method and derived semi-empirical schemes

In the following,  $p, q, r, s \dots$  refer to molecular orbitals (MOs),  $i, j, k, l \dots$  to occupied,  $a, b, c, d \dots$  to unoccupied ones, and  $\alpha, \beta, \gamma, \delta \dots$  to atomic orbitals (AOs). Within the HF framework, getting the approximated ground state wave function requires to compute two-electron integrals of the form  $(pp|qq)$  and  $(pq|qp)$ , which are Coulomb and exchange integrals, respectively, written in the Mulliken notation. Molecular orbitals are described as linear combination of atomic orbitals (LCAO), generally using contractions of Gaussian basis functions for performance reasons.

The evaluation of Coulomb and exchange integrals is obtained by the four-index transformation of AO two-electron integrals which is the computational bottleneck that precludes the application of the HF method to large systems. To overcome this, three simplifications were introduced leading to the foundation of a first set of semi-empirical methods<sup>33</sup>: (i) restriction to an effective valence shell, by reducing the number of explicitly considered electrons, (ii) restriction of the basis set expansion (generally by using a minimal basis set, which limits the number of basis functions used), and (iii) neglect of some AO two-electron integrals. The latter simplification is usually based on the zero differential overlap (ZDO) approximation<sup>34</sup> where three- and four-center AO integrals (i.e., integrals where three or four basis functions belong to different atoms) are totally neglected. In 1953, Pople,<sup>35</sup> proposed following acronyms to describe a hierarchy of (two-center) integral approximations: (i) complete neglect of differential overlap (CNDO), (ii) intermediate neglect of differential overlap (INDO), and (iii) neglect of diatomic differential overlap (NDDO). The CNDO scheme uses the ZDO approximation, so that only AO integrals  $(\alpha_A \alpha_A | \beta_B \beta_B)$  are accounted for considering that the  $\alpha$  AO is centered on atom A and the  $\beta$  AO on atom B. The INDO scheme also uses the ZDO approximation except for 1-center AO integrals where  $(\alpha_A \beta_A | \gamma_A \delta_A)$  are used. Finally, the NDDO approximation includes all  $(\alpha_A \beta_A | \gamma_B \delta_B)$  integrals.<sup>33,36</sup>

Following this, three families of methods emerged: the first one is due to the group of Zerner and coworkers and is called ZINDO.<sup>37</sup> The ZINDO/S method was designed for the calculation of electronic spectra based on a ZINDO/1 ground state. Such spectra are computed via the configuration interaction (CI) method, considering only a small subset of singly-excited determinants in a restricted active space. The second one is called the MNDO<sup>38</sup> (Modified Neglected of Diatomic overlap) method which is based on the NDDO approximation. After different reparameterization, the

MNDO scheme led to, for example, the popular AM1<sup>39</sup> and PM3<sup>40</sup> methods. The inclusion of  $d$  functions provided, for example, the MNDO/d<sup>41</sup> and PM6<sup>42</sup> methods. A last family of methods is known as orthogonalization-corrected models (OMx,  $1 \leq x \leq 3$ ), which account and correct for the orthogonalization of the Fock matrix, while also considering some three-center terms. In some flavors, effective core potentials (ECPs) are also used.<sup>43,44</sup>

The implementation of such semi-empirical models requires the evaluation of the remaining nonvanishing integrals. It is done either by using their analytical expressions, values extracted from experimental data (e.g., ionization potentials or spectroscopic data) or by using parametric expressions. For example, MNDO-type methods rely on a multipole expansion for the calculation of two-center two-electrons integrals, which are then expanded in Klopman-like approximated expressions.<sup>45</sup> Parameters are generally obtained by fitting reference data from high-level ab-initio calculations or experiment.<sup>44,46</sup>

## 2.2 | Density functional theory, density functional based tight binding, and xTB

Considering Hohenberg and Kohn<sup>47</sup> theorems, DFT emerged as an alternative to wave function methods. In Kohn and Sham formulation<sup>48</sup> of DFT, the electron density  $\rho$  is used to compute the ground state energy of a system:

$$E[\rho] = E_{\text{NN}} + V_{\text{ext}}[\rho] + F_{\text{KS}}[\rho], \quad (1)$$

$$\text{with } F_{\text{KS}}[\rho] = T_{\text{S}}[\rho] + J[\rho] + E_{\text{XC}}[\rho], \quad (2)$$

where  $E_{\text{NN}}$  is the nuclei–nuclei potential energy and  $V_{\text{ext}}$ , the nuclei–electron potential energy. Then, grouped in the Kohn–Sham (KS) functional is  $J[\rho]$ ; the Coulomb energy,  $T_{\text{S}}[\rho]$ , the kinetic energy for non-interacting electrons, and  $E_{\text{XC}}$ , which gathers unknown parts of the kinetic and potential energy terms. The latter term is described by the so-called exchange–correlation functional (XCF), which is the cornerstone of KS-DFT. Many XCFs have been developed over the past decades, based on different underlying assumptions. Among them, hybrid XCFs that include some amount of exact HF exchange were recognized to improve globally the accuracy of the method<sup>49,50</sup> in particular, when this amount could vary with the distance (range-separated hybrid XCFs).<sup>51</sup> Van der Waals interactions are usually not well captured by DFT. Empirical corrections have been developed to overcome this, for example, DFT-Dx ( $2 \leq x \leq 4$ ) schemes.<sup>52–55</sup>

Because the scaling of KS-DFT is comparable to the HF one ( $N^3$ , where  $N$  is the number of basis functions), it remains cumbersome for large systems with many ( $>500$ ) basis functions. The density functional based tight binding (DFTB) approach was developed as a semi-empirical method using a tight-binding formulation of DFT. In DFTB, the ground state density is assumed to be the sum of a reference density ( $\rho_0$ ) and a deviation from this reference density ( $\Delta\rho$ ),<sup>56,57</sup>

$$\rho = \rho_0 + \Delta\rho \quad \text{with} \quad \rho_0 = \sum_A \rho_0^A, \quad (3)$$

where  $\rho_0$  is generally chosen as the superposition of neutral atom densities,  $\rho_0^A$ . Therefore, the energy expressed as a power expansion of the ground state density becomes

$$E[\rho] = E^{(0)}[\rho_0] + E^{(1)}[\rho_0, \delta\rho] + E^{(2)}[\rho_0, (\delta\rho)^2] + E^{(3)}[\rho_0, (\delta\rho)^3] + \dots \quad (4)$$

The truncation of this expression leads to different DFTB flavors: DFTB1 scheme<sup>58</sup> only includes linear terms, DFTB2<sup>59</sup> (or SCC-DFTB) scheme truncates after the third term, and DFTB3<sup>60</sup> scheme includes the third-order term as well.

In 2016, Grimme and Bannwarth<sup>61</sup> introduced the xTB variant of DFTB to generate the ground state for ultra-fast excited state calculations. This approach is combining two different special purpose valence tight-binding (VTB) and extended tight-binding Hamiltonians (see Figure 2 for a schematic overview). A minimal valence basis set (VBS) is used with the VTB Hamiltonian in a self-consistent charge (SCC) procedure to obtain CM5-type charges that serve as input for the xTB Hamiltonian. Then, an extended AO basis set (XBS) with diffuse functions on hydrogen atoms and main

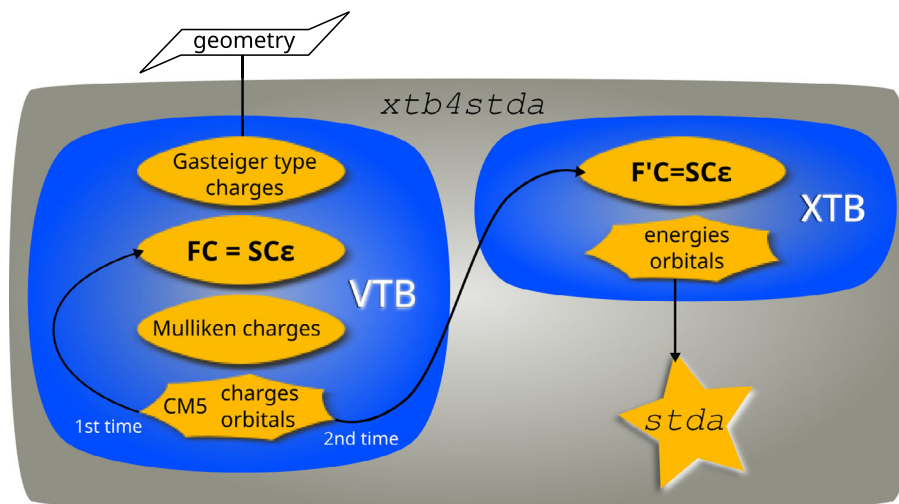


FIGURE 2 Workflow to obtain the xTB ground state.

TABLE 1 Description of the atomic orbital basis set used to get the xTB ground state.

Element	Part	
	VBS	XBS
H, He	ns	ns, (n + 1)sp
Group I/II	nsp	nsp
B-Ne	nsp	nsp, (n + 1)sp
Al, Ga, In, Zn, Cd, Hg	nsp	nsp
Remaining group		
IV–VII non-metal	nsp, (n + 1)d	nsp, (n + 1)sp
d-block elements	nd, (n + 1)sp	nd, (n + 1)sp

Note:  $n$  describes the principal quantum number of the valence shell of the respective element.

group non-metals is used with the xTB Hamiltonian for a single diagonalization step. The xTB Hamiltonian matrix element expression is similar to the second-order SCC-DFTB one:

$$\langle \alpha | \hat{F} | \beta \rangle = \langle \alpha | \hat{H}_0 | \beta \rangle + k_q \frac{1}{2} S_{\alpha\beta} \sum_C (\Gamma_{AC} + \Gamma_{BC}) q_C^{\text{VTB}}, \quad (\alpha \in A, \beta \in B). \quad (5)$$

$H_0$  is a zeroth-order Hückel-type Hamiltonian,  $k_q$  denotes an empirical scaling parameter,  $S_{\alpha\beta}$  is an AO overlap matrix element,  $q_C^{\text{VTB}}$  is the CM5<sup>62</sup> atomic charge of atom  $C$  generated by the VTB step, and  $\Gamma_{AB}$  is a scaling function for the inter-electronic repulsion between atom  $A$  and atom  $B$ . This procedure generates orbitals and their energies as input for excited state and response calculations. Note that virtual orbital energies are shifted to mimic hybrid XCF-like characters. Table 1 presents VBS and XBS information for all elements. The xTB procedure is implemented in the xtb4stda program<sup>63</sup> freely available on GitHub.

Later on, this approach was extended to the so-called GFNi-xTB<sup>64</sup> (i from 0 to 2) family of methods to compute geometries, frequencies, and non-covalent interactions for molecules up to thousands of atoms with a similar VBS. In contrast to other tight-binding models, the GFN2-xTB scheme<sup>65</sup> avoids pair-specific parameters for, for example, hydrogen or halogen bonds, by inclusion of anisotropic effects up to second-order of the multipole expansion. The inclusion of anisotropic effects also mitigates to some extent problems with the minimal valence basis set used in this ansatz. To better describe the non-covalent interactions, GFN2-xTB uses a modified, self-consistent D4 scheme.<sup>66</sup> It was shown



that GFN2-xTB is able to fastly optimize and compute properties for large (non-covalently bounded) systems<sup>67–70</sup> and even (metallo-)proteins.<sup>71</sup>

## 2.3 | Molecular response properties

Different method are available to compute the response properties of a system with respect to an (external) perturbation. The application of a time-dependent external electric field ( $\mathbf{F}(t) = \mathbf{F}^\omega [e^{-i\omega t} + e^{i\omega t}]$ ) (oscillating at a frequency  $\omega$ ) on a molecule modifies its dipole moment:

$$\vec{\mu}(\mathbf{F}) = \vec{\mu}_0 + \Delta\vec{\mu}(\mathbf{F}), \quad \text{with} \quad \Delta\vec{\mu}(\mathbf{F}) = \vec{\alpha} \cdot \mathbf{F} + \frac{1}{2!} \vec{\beta} : \mathbf{F}^2 + \frac{1}{3!} \vec{\gamma} : \mathbf{F}^3 + \dots, \quad (6)$$

where  $\mu_0$  is the intrinsic dipole moment of the molecule,  $\vec{\alpha}$  the molecular polarizability tensor and  $\vec{\beta}$  and  $\vec{\gamma}$  the first and second hyperpolarizability ( $\gamma$ ) tensors, respectively. Because tensor components depend on field directions, it is usual to write their tensor components as

$$\alpha_{\zeta\xi}(-\omega_\sigma; \omega_1), \beta_{\zeta\xi\eta}(-\omega_\sigma; \omega_1, \omega_2) \text{ and } \gamma_{\zeta\xi\eta\nu}(-\omega_\sigma; \omega_1, \omega_2, \omega_3), \quad (7)$$

where  $\omega_\sigma = \sum_i \omega_i$  and  $\zeta, \xi, \eta$  or  $\nu$  are applied electric field directions. In this review, we assumed the “T” convention.<sup>72</sup> Depending on how static ( $\omega = 0$ ) and dynamic ( $\omega \neq 0$ ) electric fields are combined, different NLO phenomena can occur. For example, the second harmonic generation is described by  $\beta_{\zeta\xi\eta}(-2\omega; \omega, \omega)$  tensor components where the energy of the emitted photon is the sum of the degenerate energies of the two incident photons.

These quantities are related to response functions derived in the context of the time-dependent perturbation theory. The change in energy due to the application of an external electric field is given by

$$E(\mathbf{F}) = E_0 - \int_0^{\mathbf{F}} \vec{\mu}(\mathbf{F}') d\mathbf{F}'. \quad (8)$$

Computing such field-dependent energies requires only to include the time-dependent perturbation  $\hat{V}(t) = -\vec{\mu} \cdot \mathbf{F}$  into the Hamiltonian:

$$\hat{H} = \hat{H}_0 - \vec{\mu} \cdot \mathbf{F}, \quad (9)$$

where  $\hat{H}_0$  is the unperturbed Hamiltonian. Because in the time-dependent perturbation theory, the time-depend dipole moment is expressed as:

$$\begin{aligned} \mu_\zeta(t) = \mu_\zeta(0) &+ \sum_{\omega} \sum_{\eta}^{x,y,z} \langle \langle \mu_\zeta; \mu_\eta \rangle \rangle_{\omega} F_{\eta}(\omega) e^{\pm i\omega t} \\ &+ \frac{1}{2!} \sum_{\omega_1, \omega_2} \sum_{\eta, \xi}^{x,y,z} \langle \langle \mu_\zeta; \mu_\eta, \mu_\xi \rangle \rangle_{\omega_1, \omega_2} F_{\eta}(\omega_1) F_{\xi}(\omega_2) e^{\pm i(\omega_1 + \omega_2)t} + \dots, \end{aligned} \quad (10)$$

polarizabilities and first hyperpolarizabilities tensor components are directly related to the linear and quadratic response functions, respectively:

$$\alpha_{\zeta\eta}(-\omega_\sigma; \omega_1) = \langle \langle \mu_\zeta; \mu_\eta \rangle \rangle_{\omega}, \quad (11)$$

$$\beta_{\zeta\eta\xi}(-\omega_\sigma; \omega_1, \omega_2) = \langle \langle \mu_\zeta; \mu_\eta, \mu_\xi \rangle \rangle_{\omega_1, \omega_2}. \quad (12)$$

Other quantities can also be derived from response functions, for example, the 2PA. In the degenerate case ( $\omega_1 = \omega_2$ ), the two-photon transition moments  $M_{\zeta\eta}^{0 \rightarrow n}$  can be derived at the pole of the quadratic response function  $\langle\langle \mu_\xi; \mu_\zeta, \mu_\eta \rangle\rangle_{\omega, \omega}$  as its single residue<sup>73</sup>:

$$\lim_{2\omega \rightarrow \omega_n} (2\omega - \omega_n) \beta_{\xi\zeta\eta}(-2\omega, \omega, \omega) = -M_{\zeta\eta}^{0 \rightarrow n} \langle 0 | \mu_\xi | n \rangle. \quad (13)$$

In practice, different methods exist to evaluate response functions and their poles.

### 2.3.1 | Finite-field approach

Derivations of the energy with respect to electric field components are always possible. Then, tensor components read

$$\alpha_{\zeta\xi} = \left( \frac{\partial^2 E}{\partial \mathbf{F}_\zeta \partial \mathbf{F}_\xi} \right)_0, \quad (14)$$

$$\beta_{\zeta\xi\eta} = \left( \frac{\partial^3 E}{\partial \mathbf{F}_\zeta \partial \mathbf{F}_\xi \partial \mathbf{F}_\eta} \right)_0, \quad (15)$$

$$\gamma_{\zeta\xi\eta\nu} = \left( \frac{\partial^4 E}{\partial \mathbf{F}_\zeta \partial \mathbf{F}_\xi \partial \mathbf{F}_\eta \partial \mathbf{F}_\nu} \right)_0, \dots \quad (16)$$

In practice, these derivatives can be evaluated numerically, applying finite-difference expressions for Equations (14)–(16), which requires to compute the energy (or lower-order properties) for different electric field amplitudes. Note that the finite field (FF) method is limited to the static case. The amplitude of the field should be chosen carefully because: (i) if too small, it could give rise to numerical errors, and (ii) if too large, the result could be contaminated by higher-order derivatives and/or other states than the ground state could be populated. While the first cause of error is inherent to any iterative quantum chemistry methods ( $\Delta\chi \propto \Delta E \times F^{-d}$ , where  $\Delta\chi$  and  $\Delta E$  are the accuracy on the resulting tensor and the energy values, respectively, and  $d$  the order of the derivative), the error from the contamination from higher order derivatives can be minimized thanks to the Richardson extrapolation (or Romberg, in the quantum chemistry community) scheme.<sup>74</sup> Thus, Mohammed et al.<sup>75</sup> established a range of acceptable field strengths, and one of us<sup>76</sup> later described an automatic procedure to analyze Romberg's triangles. Nevertheless, the FF method requires a fair amount of (single point) calculations which may not be easy to converge to the accuracy required for stable numerical derivatives.

### 2.3.2 | Sum-over-states method

Time-dependent perturbation theory can be used to compute response properties. Starting from the exact wave function, Orr and Ward<sup>77,78</sup> derived the so-called sum-over-states (SOS) expressions that give any  $n$ -order optical property tensor component:

$$\chi_{\zeta\xi\eta\dots}^{(n)}(-\omega_\sigma; \omega_1, \dots) = \sum_{\mathcal{P}} \sum_{a_1, a_2, \dots} \frac{\mu_{0a_1}^\zeta \bar{\mu}_{a_1 a_2}^\xi \dots \mu_{a_{n-1} 0}^\eta}{(\hbar\omega_{a_1} - \hbar\omega_\sigma)(\hbar\omega_{a_2} - \hbar\omega_\sigma - \hbar\omega_1) \dots}, \quad (17)$$

where  $\zeta, \xi, \eta, \dots$  are Cartesian coordinates,  $\omega_1, \omega_2, \dots$ , their corresponding pulsations,  $a_1, a_2, \dots$  number excited states of the system,  $\hbar\omega_{a_i}$  their excitation energies, and  $\sum_{\mathcal{P}}$  is the sum over different permutations of each pair  $(i, \omega_\sigma), \dots$ . Here,  $\bar{\mu}_{a_i, a_j}^\zeta = \langle a_i | \zeta | a_j \rangle - \delta_{a_i a_j} \langle 0 | \zeta | 0 \rangle$ , corresponds to the transition dipole moment from state  $a_i$  to  $a_j$ . Considering approximate wave functions, this approach can be used with any methods that compute excited states. This normally requires



to compute all excited states but usually the space of excitations is truncated at a point that allows SOS expressions to reach convergence.<sup>79–81</sup>

### 2.3.3 | Time-dependent density functional theory

Linear and nonlinear response functions can also be obtained analytically, for example, by the time-dependent HF method<sup>15,82</sup> or the time-dependent DFT (TD-DFT).<sup>83</sup> With respect to the FF method, such analytical derivations give access to dynamic properties. It also avoids truncation convergence problems inherent to any SOS expressions as well as the burden of computing large number of excited states. Here, we focus on TD-DFT, which can be routinely applied to systems up to 200 atoms nowadays.

When applying an external electric field  $\mathbf{F}$  at a frequency  $\omega$ , the full TD-DFT non-Hermitian eigenvalue problem is obtained by the Casida's equations<sup>83</sup> assuming real orbitals:

$$\left[ \begin{pmatrix} \mathbf{A} & \mathbf{B} \\ \mathbf{B} & \mathbf{A} \end{pmatrix} - \omega \begin{pmatrix} 1 & 0 \\ 0 & -1 \end{pmatrix} \right] \begin{pmatrix} \mathbf{X}_\zeta(\omega) \\ \mathbf{Y}_\zeta(\omega) \end{pmatrix} = \begin{pmatrix} \mu_\zeta \\ \mu_\zeta \end{pmatrix}, \quad (18)$$

where  $\mathbf{A}$  and  $\mathbf{B}$  are orbital rotation Hessian super-matrices and  $\mathbf{X}_\zeta(\omega)$  and  $\mathbf{Y}_\zeta(\omega)$  frequency dependent linear response vectors. These equations are transformed into a linear system:

$$[(\mathbf{A} + \mathbf{B}) - \omega^2(\mathbf{A} - \mathbf{B})^{-1}] [\mathbf{X}_\zeta(\omega) + \mathbf{Y}_\zeta(\omega)] = -2\mu_\zeta, \quad (19)$$

which is solved to obtain linear response vectors. Excitation and deexcitation vectors can be used to compute components of the polarizability tensor:

$$\alpha_{\zeta\eta}(-\omega; \omega) = -2 \sum_{ai} \mu_{\zeta,ai} (X_{\eta,ai}(\omega) + Y_{\eta,ai}(\omega)). \quad (20)$$

Switching off the dipolar perturbation into Casida's equations allows to determine excited states and their energies:

$$\begin{pmatrix} \mathbf{A} & \mathbf{B} \\ \mathbf{B} & \mathbf{A} \end{pmatrix} \begin{pmatrix} \mathbf{X} \\ \mathbf{Y} \end{pmatrix} = \begin{pmatrix} \omega & 0 \\ 0 & -\omega \end{pmatrix} \begin{pmatrix} \mathbf{X} \\ \mathbf{Y} \end{pmatrix}. \quad (21)$$

$\omega$  are excitation energies and  $\mathbf{X}$  and  $\mathbf{Y}$ , the eigenvectors. Because we consider only real orbitals, the full TD-DFT problem (Equation (21)) can be rewritten as an Hermitian eigenvalue problem:

$$\begin{aligned} (\mathbf{A} - \mathbf{B})^{\frac{1}{2}} (\mathbf{A} - \mathbf{B})(\mathbf{A} - \mathbf{B})^{\frac{1}{2}} \mathbf{Z} &= \omega^2 \mathbf{Z}, \\ \text{with } \mathbf{Z} &= (\mathbf{A} - \mathbf{B})^{\frac{1}{2}} (\mathbf{X} + \mathbf{Y}). \end{aligned} \quad (22)$$

For a global hybrid density functional, the elements of  $\mathbf{A}$  and  $\mathbf{B}$  super-matrices are written as:

$$A_{ia,jb} = \delta_{ij} \delta_{ab} (\epsilon_a - \epsilon_i) + 2(ia|jb) - a_x (ij|ab) + (1 - a_x) (ia|f_{XC}|jb), \quad (23)$$

$$B_{ia,jb} = 2(ia|bj) - a_x (ib|aj) + (1 - a_x) (ia|f_{XC}|bj), \quad (24)$$

where  $\epsilon_i$  and  $\epsilon_a$  are orbital energies,  $a_x$  is the amount of non-local Fock exchange into the exchange-correlation functional,  $(ia|jb)$ ,  $(ia|bj)$ , and  $(ib|aj)$  are exchange-type and  $(ij|ab)$  Coulomb-type two-electron integrals,  $(ia|f_{XC}|jb)$  and

( $ia|f_{XC}|bj$ ) are responses of the exchange-correlation functional. The time-dependent exchange-correlation kernel  $f_{XC}$  is usually derived from the time-independent exchange-correlation functional applying the adiabatic approximation.

Considering two incident photons, the quadratic-response (QR) TD-DFT equations should be solved to obtain the quadratic response function  $\beta_{\xi\eta\xi}(-\omega_\sigma; \omega_1, \omega_2)$ . To circumvent the cost of directly computing the quadratic response, the  $2n+1$  theorem<sup>84,85</sup> is used to rewrite QR TD-DFT equations in term of frequency-dependent linear response vectors for three different frequencies (incident photon frequencies  $\omega_1$  and  $\omega_2$  and the emitted photon frequency,  $-\omega_\sigma = -\omega_1 - \omega_2$ ):

$$\beta_{\xi\eta\xi}(-\omega_\sigma; \omega_1, \omega_2) = A - B + C, \quad (25)$$

with

$$A = \sum_{perm.\xi,\zeta,\eta} \left\{ \sum_{aij} X_{\xi,ai}(-\omega_\sigma) \left[ -\mu_{\zeta,ij} + \sum_{ck} f_{ij,ck}^{HXC} (X_{\zeta,ck}(\omega_1) + Y_{\zeta,ck}(\omega_1)) \right] Y_{\eta,aj}(\omega_2) \right\}, \quad (26)$$

$$B = \sum_{perm.\xi,\zeta,\eta} \left\{ \sum_{iab} X_{\xi,ai}(-\omega_\sigma) \left[ -\mu_{\zeta,ab} + \sum_{ck} f_{ab,ck}^{HXC} (X_{\zeta,ck}(\omega_1) + Y_{\zeta,ck}(\omega_1)) \right] Y_{\eta,bi}(\omega_2) \right\}, \quad (27)$$

$$C = \sum_{perm.\xi,\zeta,\eta} \left\{ \sum_{aibjck} g_{ai,bj,ck}^{XC} [X_{\xi,ai}(-\omega_\sigma) + Y_{\xi,ai}(-\omega_\sigma)] [X_{\zeta,bj}(\omega_1) + Y_{\zeta,bj}(\omega_1)] [X_{\eta,ck}(\omega_2) + Y_{\eta,ck}(\omega_2)] \right\}. \quad (28)$$

where  $perm.\xi,\zeta,\eta$  is the permutational sum over six different perturbations and  $f_{ij,ck}^{HXC}$  are elements of the combined Hartree exchange-correlation kernel:

$$f_{ij,ck}^{HXC} = 2(ij|ck) - a_x(jk|ci) + (1 - a_x)(ij|f_{XC}|ck). \quad (29)$$

$g_{ai,bj,ck}^{XC}$  are matrix elements of the third functional derivative of the exchange-correlation functional. To compare to experimental values (which are usually obtained by hyper-Rayleigh scattering experiments for second-harmonic generation,  $\beta_{\xi\zeta\eta}(-2\omega; \omega, \omega)$ ), the theoretical  $\beta_{HRS}$  value is obtained as the mean of  $\beta$ -tensor orientations<sup>8</sup>:

$$\beta_{HRS}(-2\omega; \omega, \omega) = \sqrt{\langle \beta_{ZZZ}^2 \rangle + \langle \beta_{ZXX}^2 \rangle}, \quad (30)$$

whereas  $\langle \beta_{ZZZ}^2 \rangle$  and  $\langle \beta_{ZXX}^2 \rangle$  are obtained without assuming Kleinman's condition<sup>86</sup> in the laboratory frame ( $X$ ,  $Y$ , and  $Z$ ). Note that for the static  $\beta$ , that is, when  $\omega \rightarrow 0$ , Kleinman's conditions<sup>86</sup> are used because they are strictly exact in this case. Consequently, the computational cost is reduced to the evaluation of only 10 tensor components.

### 2.3.4 | Simplified TD-DFT

In 2013, to provide a computationally efficient TD-DFT scheme that better balances cost and accuracy, Grimme<sup>87</sup> introduced simplifications to TD-DFT considering the Tamm-Dancoff approximation (TDA),<sup>88</sup> resulting in a method called simplified TDA (sTDA). A year later, the same simplifications were applied to TD-DFT, leading to the sTD-DFT method.<sup>89</sup> Originally, these methods were used to compute only UV-Vis and circular dichroism (CD) spectra.

Three main simplifications were applied to Equation (22). First, integrals involving the time-dependent exchange-correlation functional  $f_{XC}$  in **A** and **B** super-matrices are neglected.

Second, the singly-excited ( $i \rightarrow a$ ) configuration space is truncated considering a single energy threshold  $E_{\text{thresh}}$ . The active MO space is defined between  $\epsilon_{\min} = \epsilon_{\text{HOMO}} - 2(1 + 0.8a_x)E_{\text{thresh}}$  and  $\epsilon_{\max} = \epsilon_{\text{LUMO}} + 2(1 + 0.8a_x)E_{\text{thresh}}$ . Then, a first set of primary configuration state functions (P-CSFs) is selected considering that  $A_{ia,ia} \leq E_{\text{thresh}}$ . Configurations

( $j \rightarrow b$  with  $A_{jb,jb} > E_{\text{thresh}}$ ) that presents a second-order perturbation energy  $E_{jb}^{(2)} = \sum_{ia}^{\text{P-CSFs}} \frac{|A_{ia,jb}|^2}{A_{ia,ia} - A_{jb,jb}}$  larger than  $10^{-4}E_h$  are sorted out as secondary CSF (S-CSFs). The space of selected CSFs is the sum of both P-CSFs and S-CSFs.

Third, to evaluate two electron integrals, the ZDO approximation is considered:

$$(ia|jb) \approx \sum_{\alpha\beta} C_{ia}^{\text{low}*} C_{aa}^{\text{low}} C_{j\beta}^{\text{low}*} C_{b\beta}^{\text{low}} (\lambda_{\alpha}\lambda_{\alpha}|\lambda_{\beta}\lambda_{\beta}). \quad (31)$$

where  $C_{ia}^{\text{low}*}$  are Löwdin-orthogonalized LCAO coefficients and  $\lambda_{\alpha}$  are orthogonalized Löwdin basis functions. These basis functions are supposed to be atom centered allowing to collect transition charges for each  $A$  atom:

$$Q_A^{ia} = \sum_{\alpha \in A}^N C_{ai}^{\text{low}*} C_{aa}^{\text{low}}. \quad (32)$$

Doing so, Equation (31) can be rewritten and approximated as

$$(ia|jb) \approx \sum_{AB}^N Q_A^{ia} Q_B^{jb} (AA|BB). \quad (33)$$

where  $A$  and  $B$  denote atoms and  $N$  is the total number of atoms in the system. In sTDA and sTD-DFT methods, the four-index two-electron integrals ( $pq|rs$ ) in Equations (23) and (24) are replaced by short-range damped Coulomb interactions between atom-centered monopole charges  $Q_A^{ia}$  (calculated from a Löwdin orthogonalization<sup>90</sup>) and  $(AA|BB)$  are Mataga–Nishimoto–Ohno–Klopman (MNOK) damped Coulomb operators according to the type of integrals. For Coulomb-type integrals, it reads:

$$(AA|BB)^J = \left( \frac{1}{(R_{AB})^{y_J} + (a_x \eta)^{-y_J}} \right)^{\frac{1}{y_J}} \text{ with } \eta = \frac{\eta(A) + \eta(B)}{2}. \quad (34)$$

$R_{AB}$  denotes the distance between the two atoms  $A$  and  $B$ ,  $y_J$  is a globally-fitted parameter for a range of  $a_x$ , and  $\eta$  depends on the chemical hardness of the two atoms  $A$  and  $B$ . Tabulated  $\eta(A)$  values consistent for all elements of the periodic table are used.<sup>91</sup> For exchange-type integrals, the corresponding expression reads:

$$(AA|BB)^K = \left( \frac{1}{(R_{AB})^{y_K} + \eta^{-y_K}} \right)^{\frac{1}{y_K}}, \quad (35)$$

where  $y_K$  is another globally-fitted parameter. As different decay behaviors for Coulomb and exchange-type integrals are used, their physically different origins are emphasized.  $y_K$  and  $y_J$  were globally adjusted to reproduce reference excitation energies.<sup>87</sup> Consequently, the neglect of the  $f_{XC}$  response is mitigated to some extent by these adjustments. Applying these simplifications, **A** and **B** are approximated as:

$$A'_{ia,jb} = \delta_{ij} \delta_{ab} (\epsilon_a - \epsilon_i) + \sum_{A,B}^N \left( 2Q_A^{ia} Q_B^{jb} (AA|BB)^K - Q_A^{ij} Q_B^{ab} (AA|BB)^J \right), \quad (36)$$

$$B'_{ia,jb} = \sum_{A,B}^N \left( 2Q_A^{ia} Q_B^{bj} (AA|BB)^K - a_x Q_A^{ib} Q_B^{aj} (AA|BB)^K \right). \quad (37)$$

Starting in 2018, de Wergifosse and coworkers<sup>22,24,92–94</sup> extended the reach of the sTD-DFT framework to response properties, allowing the computation of the polarizability,<sup>92</sup> optical rotation,<sup>93</sup> first hyperpolarizability,<sup>92</sup> excited state

absorption,<sup>24</sup> and two-photon absorption.<sup>94</sup> To obtain sTD-DFT frequency-dependent linear response vectors, **A** and **B** are replaced in Equation (19) by their sTD-DFT counterparts (Equations (36) and (37)):

$$\left[ \mathbf{X}'_{\zeta}(\omega) + \mathbf{Y}'_{\zeta}(\omega) \right] \left[ (\mathbf{A}' + \mathbf{B}') - \omega^2 (\mathbf{A}' - \mathbf{B}')^{-1} \right] = -2\mu_{\zeta}. \quad (38)$$

Linear response vectors can be used to determine components of the polarizability tensor:

$$\alpha'_{\zeta\eta}(-\omega; \omega) = -2 \sum_{ai} \mu_{\zeta,ai} \left( X'_{\eta,ai}(\omega) + Y'_{\eta,ai}(\omega) \right), \quad (39)$$

as well as for the optical rotation tensor:

$$\mathfrak{F} \langle \langle m_a; \mu_a \rangle \rangle'_{\omega} = \mathfrak{F} \left( 2\omega \sum_{ia,jb} m_a (A' - B')^{-1}_{ia,jb} \left( X'_{a,jb}(\omega) + Y'_{a,jb}(\omega) \right) \right). \quad (40)$$

To compute  $\beta$  efficiently in the sTD-DFT framework,<sup>92</sup> two extra simplifications to Equation (25) are necessary: the neglect of the response of the exchange-correlation kernel (Equation (28)) and the Hartree exchange-correlation kernel (terms involving  $f^{HXC}$  in Equations (26) and (27)), leading to the following expression:

$$\beta'_{\xi\zeta\eta}(-2\omega; \omega, \omega) = A' - B', \quad (41)$$

with

$$A' = \sum_{perm.\xi,\zeta,\eta} \left\{ \sum_{aij} X'_{\xi,ai}(-2\omega) \left[ -\mu_{\zeta,ij} \right] Y'_{\eta,aj}(\omega) \right\}, \quad (42)$$

$$B' = \sum_{perm.\xi,\zeta,\eta} \left\{ \sum_{iab} X'_{\xi,ai}(-2\omega) \left[ -\mu_{\zeta,ab} \right] Y'_{\eta,bi}(\omega) \right\}. \quad (43)$$

Note that due to these approximations only the unrelaxed  $\beta$  tensor is computed with the sTD-DFT method, neglecting orbital relaxation effects. Nevertheless, de Wergifosse and Grimme<sup>92</sup> showed that neither approximations influence drastically the  $\beta$  values of push-pull  $\pi$ -conjugated systems while speeding up calculations by a factor of about 100. Note that presently, only the second harmonic generation (SHG) case is implemented in the stda program,<sup>87</sup> that is, both incident photons are of the same frequency ( $\omega_1 = \omega_2$ ).

From the single residue (Equation (13)) of the sTD-DFT first hyperpolarizability (Equation (41)), sTD-DFT two-photon transition moments<sup>94</sup> are computed as:

$$M^{0 \rightarrow n}_{\zeta\eta} = -A' + B', \quad (44)$$

with

$$A' = \sum_{perm.\xi,\zeta,\eta} \left\{ \sum_{aij} X'_{n,ai} \left[ \mu_{\zeta,ij} (1 - \delta_{\zeta n}) \right] Y'_{\eta,aj}(-\omega_n/2) \right\}, \quad (45)$$

and

$$B' = \sum_{perm.\xi,\zeta,\eta} \left\{ \sum_{iab} X'_{n,ai} [\mu_{\zeta,ab}(1 - \delta_{\zeta n})] Y'_{\eta,bi}(-\omega_n/2) \right\}. \quad (46)$$

The rotationally averaged 2PA strength<sup>95,96</sup>  $\langle \delta^{2PA} \rangle$  reads

$$\langle \delta^{2PA} \rangle = \frac{F}{30} \sum_{\zeta,\eta} S_{\zeta\zeta,\eta\eta} + \frac{G}{30} \sum_{\zeta,\eta} S_{\zeta\eta,\zeta\eta} + \frac{H}{30} \sum_{\zeta,\eta} S_{\zeta\eta,\eta\zeta}, \quad \text{with } S_{\zeta\eta,\xi\nu} = M_{\zeta\eta}^{0 \rightarrow n} M_{\xi\nu}^{0 \rightarrow n}. \quad (47)$$

For parallel linearly polarized incident light, parameters  $F$ ,  $G$ , and  $H$  are all equal 2. From Equation (47), the macroscopic two-photon absorption cross section  $\sigma^{2PA}$  reads

$$\sigma^{2PA} = \frac{N\pi^3\alpha\alpha_0^5(2\omega)^2}{c} \langle \delta^{2PA} \rangle S(2\omega, \omega_n, \Gamma), \quad (48)$$

employing a parameter  $N$  to account for different types of experimental conditions (single beam or double beam) as well as a line-shape function  $S(2\omega, \omega_n, \Gamma)$  (Gaussian or Lorentzian). Note that the macroscopic  $\sigma^{2PA}$  depends on the computed excitation energy ( $\sigma^{2PA} \propto (2\omega)^2$ ). Therefore, errors in the computation of excitation energies impact macroscopic cross-sections  $\sigma^{2PA}$ .

From the double residue of the quadratic response

$$\lim_{\omega_b \rightarrow -\omega_m} \lim_{\omega_m \omega_c \rightarrow \omega_n} (\omega_b + \omega_m)(\omega_c - \omega_n) \beta_{\xi\xi\eta}(-(\omega_b + \omega_c); \omega_b, \omega_c) = -\langle 0 | \mu_\xi | m \rangle \langle m | \mu_\xi - \langle 0 | \mu_\xi | 0 \rangle | n \rangle \langle n | \mu_\eta | 0 \rangle, \quad (49)$$

the sTD-DFT unrelaxed singlet-state-to-singlet-state transition dipole moment<sup>24</sup> can be extracted:

$$\langle m | \mu_\xi - \langle 0 | \mu_\xi | 0 \rangle | n \rangle = \frac{1}{2} \left\{ \sum_{aij} [X'_{ia} \mu_{ij,\xi} X'_{ja}^m + Y'_{ia} \mu_{ij,\xi} Y'_{ja}^n] - \sum_{abi} [X'_{ia} \mu_{ab,\xi} X'_{bi}^m + Y'_{ia} \mu_{ab,\xi} Y'_{bi}^n] \right\}, \quad (50)$$

as well as in the sTDA framework<sup>24</sup>:

$$\langle m | \mu_\xi - \langle 0 | \mu_\xi | 0 \rangle | n \rangle_{TDA} = \frac{1}{2} \left\{ \sum_{aij} [X'_{ia} \mu_{ij,\xi} X'_{ja}^m] - \sum_{abi} [X'_{ia} \mu_{ab,\xi} X'_{bi}^m] \right\}. \quad (51)$$

Excited-state absorption (ESA) spectra in the dipole-length formalism can be computed using state-to-state oscillator strengths defined as

$$f_{mn} = \frac{2}{3} (\omega_m - \omega_n) \vec{\mu}_{mn} \cdot \vec{\mu}_{nm}. \quad (52)$$

The computational bottleneck for sTD-DFT/sTDA methods is the construction of  $\mathbf{A}'$  and  $\mathbf{B}'$  super-matrices that directly depends on the number of CSFs included in by the CI space truncation procedure. To treat large systems with central chromophores efficiently such as fluorescent proteins, Beaujean et al.<sup>27</sup> introduced the dual-threshold sTD-DFT (dt-sTD-DFT) method. The idea is to use a larger number of CSFs for parts of the system mostly responsible for the response such as the chromophore. After the truncation of the MO space as for the single threshold procedure between  $\epsilon_{\min} = \epsilon_{\text{HOMO}} - 2(1 + 0.8a_x)E_{\text{high}}$  and  $\epsilon_{\max} = \epsilon_{\text{LUMO}} + 2(1 + 0.8a_x)E_{\text{high}}$ , the system is divided in two parts: a high level part and a low level one. Occupied MOs that belong to the high level part have more than 10% of their density on atoms from this part:

$$\zeta_i = \sum_{\alpha \in \text{high level}} C_{\alpha i}^2, \quad (53)$$

$$\zeta_i > 0.1 \rightarrow E_{\text{high}}, \quad (54)$$

$$\zeta_i \leq 0.1 \rightarrow E_{\text{low}}. \quad (55)$$

They are involved in the procedure considering a first energy threshold called  $E_{\text{high}}$ . Remaining occupied MOs are treated with a second energy threshold  $E_{\text{low}}$ . First, singly-excited ( $i_{\text{high}} \rightarrow a$ ) CSFs are selected as primary CSFs for the high level part (P-CSFs-H) if  $A_{ia,ia} \leq E_{\text{high}}$ . Second, in the same manner, singly-excited ( $i_{\text{low}} \rightarrow a$ ) CSFs are accounted for as primary CSFs for the low level part (P-CSFs-L) if  $A_{ia,ia} \leq E_{\text{low}}$ . If the second-order perturbation contribution  $E_{jb}^{(2)} = \sum_{ia}^{\text{P-CSFs-(H+L)}} \frac{|A_{ia,jb}|^2}{A_{ia,ia} - A_{jb,jb}}$  of a remaining singly-excited ( $j \rightarrow b$ ) CSF for  $A_{j_{\text{high}}b, j_{\text{high}}b} > E_{\text{high}}$  or  $E_{\text{low}} < A_{j_{\text{low}}b, j_{\text{low}}b} < 2(1 + 0.8a_x)E_{\text{low}}$  is lower than  $10^{-4}E_h$  then they are selected as S-CSFs. The configuration space is the sum of P-CSFs-H, P-CSFs-L, and S-CSFs.

In summary, the sTD-DFT method can calculate (non-)linear optical properties of large molecules. The computational bottleneck is the determination of the DFT ground state, limiting sTD-DFT excited states and response properties calculations to systems up to 1000 atoms. Using the xTB method for the ground state calculation extends the reach of simplified methods to very large systems with several thousands of atoms. All these implementation are available in the stda program.<sup>87</sup>

### 2.3.5 | The eXact integral sTD-DFT

In sTD-DFT, replacing two-electron integrals on the Löwdin basis ( $\lambda_\alpha \lambda_\alpha | \lambda_\beta \lambda_\beta$ ) by parameter-dependent MNOK damped Coulomb operators ( $AA|BB$ ) can be seen as a physically-sounded but crude approximation that does not depend anymore on basis functions involved. Alternatively, two-electron integrals on the Löwdin basis ( $\lambda_\alpha \lambda_\alpha | \lambda_\beta \lambda_\beta$ ) could be simply replaced by their AO counterparts ( $\alpha\alpha|\beta\beta$ ), leading to the following approximation to evaluate MO two-electron integrals:

$$(ia|jb) \approx \sum_{\alpha\beta} C_{ia}^{\text{low}*} C_{aa}^{\text{low}} C_{j\beta}^{\text{low}*} C_{b\beta}^{\text{low}} (\alpha\alpha|\beta\beta). \quad (56)$$

Collecting AO transition charges

$$Q_\alpha^{ia} = \sum_a C_{ai}^{\text{low}*} C_{aa}^{\text{low}}, \quad (57)$$

this expression can be made computationally efficient by precomputing

$$(ia|\beta\beta) = \sum_\alpha Q_\alpha^{ia} (\alpha\alpha|\beta\beta), \quad (58)$$

and then taking the dot product that scales with the number of AOs:

$$(ia|jb) \approx \sum_\beta (ia|\beta\beta) Q_\beta^{jb}. \quad (59)$$

This is the foundation of the XsTD-DFT method for which the semi-empiricism of the sTD-DFT method is removed. With respect to the sTD-DFT scheme, the approximate evaluation of MO two-electron integrals scales with the number of basis functions instead of the number of atoms, but remains computationally efficient with respect to the full scheme. For example, computing 1204 excited states with the sTDA scheme for a perylene-3,4,9,10-tetracarboxylic bisimide



derivative (60 atoms) took 14 s on a 8 CPUs (Intel Xeon CPU E5-2660 v4, 3.2 GHz) desktop computer and 3.85 min for 1121 states using the XsTDA approach, considering  $E_{\text{thresh.}} = 10$  eV. To compute 20 excited states at the B3LYP/6-31 + G(d) (TDA) level of theory for this system took 26.50 min on the same desktop computer. A full paper on this subject is under preparation by one us and should be soon submitted for publication. It must be noted that in comparison to sTD-DFT, the XsTD-DFT method can provide improved excitation energies and oscillator strengths with respect to TD-DFT as well as faithfully reproduced first hyperpolarizability frequency dispersions. More details will be provided soon.

### 2.3.6 | Solvent effects

While simplified methods can deal with large systems and thus account explicitly for the impact of the environment, it might still be necessary to account for an outer layer of surroundings, for example, to model solvent effects. This can be achieved in different manners. Currently to compute the xTB ground state, only the generalized Born/surface area<sup>97–99</sup> (GBSA) is available to account implicitly for solvent effects. The Gibbs free energy of solvation is decomposed into three terms:

$$\Delta G_{\text{solv}} = \underbrace{\Delta G_{\text{cav}} + \Delta G_{\text{vdw}}}_{\Delta G_{\text{cd}}} + \Delta G_{\text{pol}}, \quad (60)$$

where  $\Delta G_{\text{cav}}$  is the energy of the solute cavity in the solvent continuum,  $\Delta G_{\text{vdw}}$  accounts for the solute-solvent vdW interactions (dispersion), and  $\Delta G_{\text{pol}}$  is coming from the electrostatic solute-solvent interactions. The GBSA model groups the first two terms into a single one,  $\Delta G_{\text{cd}}$ , proportional to the solvent-accessible surface. The polarization term is estimated by a simple function, which interpolates between the short-range Born expression<sup>100</sup> (solvation of a spherical ion) and the long-range Coulomb behavior (described by the Poisson–Boltzmann equation).

The Polarizable Continuum Model (PCM)<sup>101,102</sup> gives a more accurate alternative to GBSA but is currently not available for the xTB ground state. It also approximates the system by placing the solute into a cavity but the procedure is self-consistent: the charge distribution of the solute polarizes the continuum, which in return polarizes the charge distribution, and so on until convergence. This is done by discretizing the solvent-accessible surface in tesserae to evaluate the potential of the cavity. The formalism has been extended to fully account for dynamic solvent effects on the different time-(in)dependent properties.<sup>103</sup>

## 3 | DISCUSSION

This section focuses on application of modern sQC methods, especially the sTD-DFT, to compute NLO properties of large systems, including the first hyperpolarizability (Section 3.1), two-photon absorption (Section 3.2), excited state absorption (Section 3.3), and second hyperpolarizability (Section 3.4). By sake of completeness, in each subsection, historical overviews of applications of early-stage semi-empirical methods to compute such properties are also given to systems that were considered large at the time. Then, modern studies that involved applications of sTD-DFT/sTDA methods to large systems are reviewed.

### 3.1 | The first hyperpolarizability

Semi-empirical computations of the first hyperpolarizability are possible since the 1960s.<sup>104</sup> At the time, such methods were applied to systems up to 30 atoms, allowing to validate structure–property relationships like it was done for the two-state approximation in 1977 for nitroanilines.<sup>105</sup> In the 1990s, studies were investigating the influence of the length of oligomers on NLO properties<sup>106</sup> as well as the response of octupolar compounds (~60 atoms).<sup>107</sup> Solvent effects<sup>108</sup> were also accounted for as well as the impact of hydrogen bonds<sup>109,110</sup> on the  $\beta$  response. One of the largest system (~150 atoms) studied in that period was a 3-methyl-4-nitroaniline crystal with the AM1 model.<sup>111</sup> Nowadays, thanks to the sTD-DFT, these boundaries are pushed away to systems up to ~5000 atoms. For clarity, this section is divided in

subsections related to the approach used to evaluate first hyperpolarizabilities, that is, FF, SOS, response functions, and sTD-DFT methods.

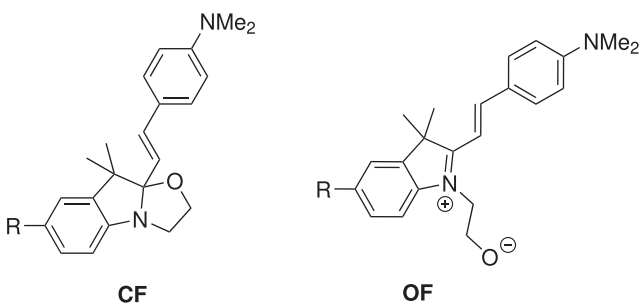
### 3.1.1 | Finite field method

In 1967, Schweig<sup>104</sup> used the FF approach for one of the first time with a Hückel Hamiltonian to compute the static first and second hyperpolarizabilities of several push-pull molecules containing up to 30 atoms. The same systems were later investigated by Zyss<sup>112–114</sup> with the INDO Hamiltonian. Following this, the development of different semi-empirical methods (CNDO, INDO, and NDDO) led to a plethora of applications considering small molecules,<sup>115</sup> polymers<sup>116,117</sup> (up to 40 carbon sites), push-pull systems<sup>118</sup> (about 50 atoms), NLO switches,<sup>119</sup> and crystals<sup>111,120</sup> (up to 150 atoms). All these studies were helped by the development of new FF subroutines such as the ones available in MOPAC,<sup>121</sup> one of the most popular implementation in the 1990s. Results generally followed experimental trends as well as those from higher-level *ab initio* calculations.

In 2013, N  non and Champagne<sup>25</sup> used the SCC-DFTB method to study the first hyperpolarizability of indolinooxazolidine molecules grafted on a SiO<sub>2</sub> surface, demonstrating the ability of this approach to deal with large systems. As shown in Figure 3, indolinooxazolidine is a NLO switch that presents different first hyperpolarizabilities in both closed and open forms. The contrast of first hyperpolarizabilities between both forms was maintained when from gas phase, it was adsorbed on the SiO<sub>2</sub> surface. The role of the linker between the chromophore and the surface was also highlighted. In 2014, N  non and Champagne<sup>122</sup> performed similar calculations on fullerene (C<sub>60</sub>) molecules grafted on two different surfaces: SiO<sub>2</sub> ( $\beta$  response of about 2000 a.u. per unit cell) and TiO<sub>2</sub> (about 8000 a.u. per unit cell). While both individual systems (fullerene and surface) do not present any first hyperpolarizability, their interaction induces a charge-transfer contribution that gives rise to a non-negligible first hyperpolarizability.

### 3.1.2 | Sum-over-states approach

While the FF approach is limited to the evaluation of the static first hyperpolarizability, the SOS approach can compute frequency-dependent first hyperpolarizabilities. Sum truncations need to be monitored carefully to avoid convergence problems with the number of excited states included in.<sup>20</sup> In the 1990s, the SOS approach was used to evaluate the first hyperpolarizability of push-pull molecules<sup>79,108,123,124</sup> and intermolecular complexes.<sup>110,125</sup> This approach was often used with INDO/S excitation energies and state-to-state transition dipole moments for which the INDO/S method was parametrized. Parameters were available for main group elements (i.e., B, N)<sup>126</sup> as well as metallic ones.<sup>80</sup> The SOS



R =	Gas phase			Adsorbed on SiO <sub>2</sub>		
	$\beta_{CF}$	$\beta_{OF}$	$\beta_{OF}/\beta_{CF}$	$\beta_{CF}$	$\beta_{OF}$	$\beta_{OF}/\beta_{CF}$
OH	1266	6877	5.4	1619	4133	2.5
Si(OH) <sub>3</sub>	1592	10 425	6.6	1552	10 351	6.7

**FIGURE 3** Sketches of indolinooxazolidine NLO switch (top), in its closed (**CF**) and open (**OF**) forms. Values (bottom) of the static  $\beta_{zzz}$  (in a.u.,  $z$  is along the C–O/Si direction for isolated compound, and normal to the surface for the adsorbed one) for the different forms and their corresponding contrasts ( $\beta_{OF}/\beta_{CF}$ ), as computed at the SCC-DFTB level.<sup>25</sup>

approach allows to decompose the response into excited state contributions, helpful for the design of new compounds with enhanced first hyperpolarizabilities.<sup>127</sup>

Nowadays, He et al.<sup>128</sup> developed LinSOSProNLO approach for the efficient computation of the first and second hyperpolarizabilities from ZINDO calculations.<sup>129</sup> They recently studied large (doped) nanographenes showing the impact of defects on the  $\beta$  response.<sup>31,32,128</sup> For example, the longitudinal  $\beta$  responses of spiral graphene nanoribbon are at least 5 times larger when defects are present (from  $\text{SGN}_n$  to  $\text{ADSGN}_n$  in Figure 4) and this effect is enhanced when increasing the number of units ( $n$ ). Together with studies on other kinds of defects,<sup>32</sup> they provided insights on new ways to create new NLO materials with enhanced  $\beta$  responses.

### 3.1.3 | Response functions, toward the sTD-DFT approach

Implementations of response functions to evaluate the first hyperpolarizability, started with the coupled-perturbed HF method, were also applied to semi-empirical Hamiltonians.<sup>82</sup> Waite, Papadopoulos and Nicolaides<sup>130–132</sup> implemented a MNDO version in the 1980s. They studied the second-order response of alkanes,<sup>130</sup> polyenes,<sup>131</sup> aromatic compounds,<sup>132</sup> and nitrogen heterocycles,<sup>133</sup> up to 30 atoms. In 1993, the first hyperpolarizability of the malachite green and rhodamine (up to 50 atoms) were investigated using a CNDO Hamiltonian.<sup>134</sup> In the 1990s, some studies compared the INDO/S and other semi-empirical results to HF showing relatively good agreements.<sup>135,136</sup> Due to the availability of TD-HF and TD-DFT implementations as well as the increasing computational power, semi-empirical methods to evaluate second-order properties started to decline in the early 21st century.

In 2018, one of us extended the reach of the sTD-DFT method to second-order response properties,<sup>92</sup> reigniting the interest in semi-empirical methods to compute first hyperpolarizabilities. Subroutines to evaluate linear and quadratic response functions were added to the stda program.<sup>87</sup> This implementation was benchmarked considering different challenging compounds, including two large systems: fluorescent protein chromophores and their first shell of residues as well as a model of collagen triple helix. The geometries as well as reference (static and dynamic)  $\beta_{\text{HRS}}$  values were taken from the literature.<sup>137–144</sup>

Among the results, the static  $\beta_{\text{HRS}}$  of three fluorescent protein chromophores (eGFP, SHardonnay, and DsRed) were computed at the sTD-DFT-xTB level and compared with HF, BHandHLYP, and MP2 calculations (Figure 5), showing an excellent comparison with MP2 results and even outperforming HF and BHandHLYP for Shardonay and DsRed. Following this, protein surrounding effects were introduced by including the first shell of residues around chromophores, increasing the system sizes to about 170 atoms, all treated again at the sTD-DFT-xTB level of theory. Static  $\beta_{\text{HRS}}$  values were compared with ONIOM MP2:HF results.<sup>138,139</sup> Figure 6 shows this excellent comparison. Note that while

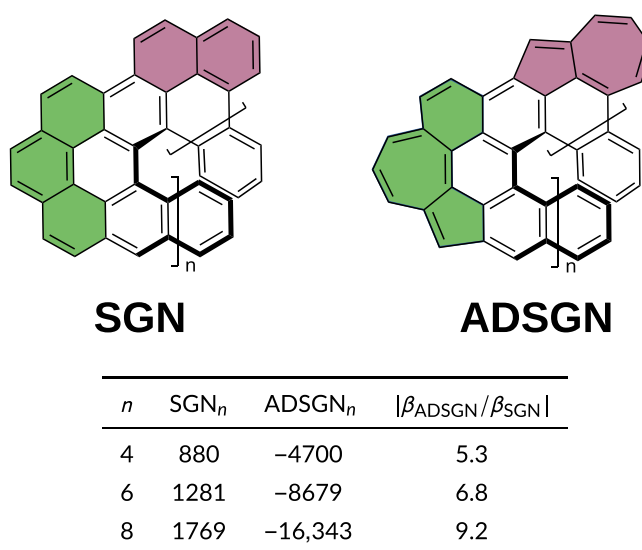


**FIGURE 4** Sketches of repetitive unit of spiral graphene nanoribbon without (top left, SGN) and with (top right, ADSGN) azulene defects. Evolution (bottom) of the static  $\beta_z = \beta_{zzz} + \frac{1}{3} \sum_i (\beta_{izz} + \beta_{ziz} + \beta_{zzi})$  (in  $10^3$  a.u.) with the number of units ( $n$ ).<sup>128</sup>  $z$  is parallel to the elongation direction of the spiral. Adapted with permission from He et al.<sup>128</sup> Copyright 2019, American Chemical Society.

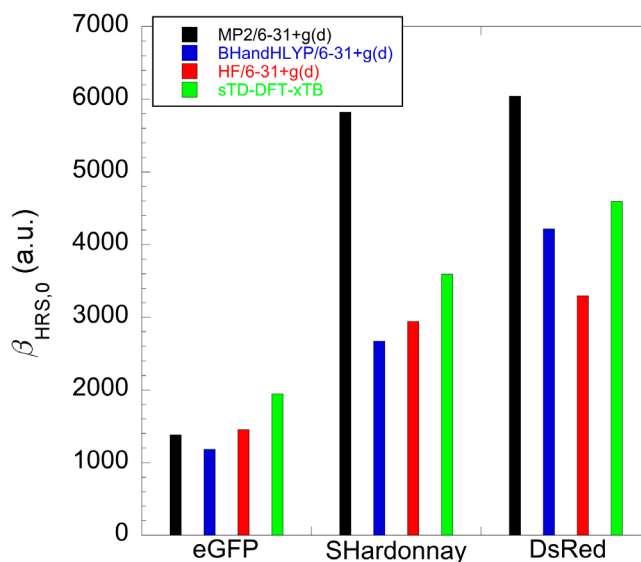


**FIGURE 5** Static  $\beta_{\text{HRS}}$  values for eGFP, SHardonnay, and DsRed chromophores obtained at the sTD-DFT-xTB level of theory and compared with HF, BHandHLYP, and MP2/6-31+G(d) reference values.<sup>92</sup> Adapted with permission from de Wergifosse and Grimme.<sup>92</sup> Copyright 2018, AIP Publishing.

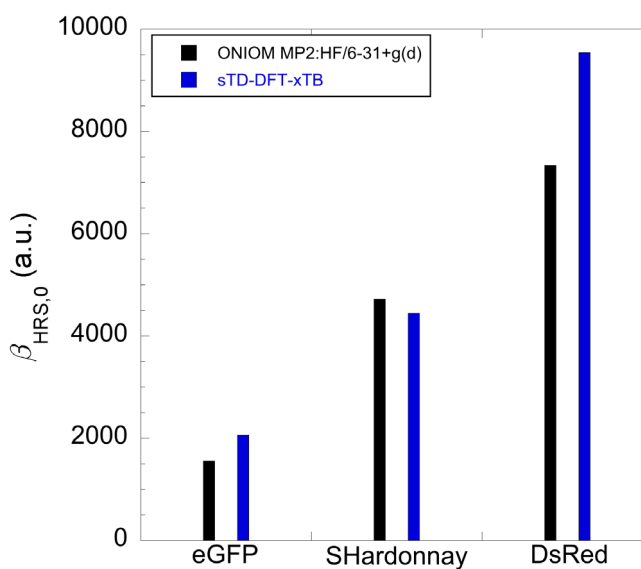


**FIGURE 6** Static  $\beta_{\text{HRS}}$  for eGFP, SHardonnay, and DsRed chromophores and their first shell of surrounding residues obtained at the sTD-DFT-xTB level of theory and compared with ONIOM MP2:HF/6-31+G(d) reference values.<sup>92</sup> Adapted with permission from de Wergifosse and Grimme.<sup>92</sup> Copyright 2018, AIP Publishing.

ONIOM calculations took several months to be completed, sTD-DFT-xTB  $\beta_{\text{HRS}}$  results were obtained within a few hours, opening the way to ultra-fast screening applications for enhanced NLO properties of large (bio-) molecules.

The largest system of this study was a collagen model (PPG10,  $\sim 1000$  atoms). The  $\beta_{\text{HRS}}$  frequency dispersion was evaluated with the sTD-DFT-xTB approach and compared with ONIOM HF/6-31+G(d):HF/6-31G(d) and ONIOM LC-BLYP/6-31+G(d):HF/6-31G(d) results. The sTD-DFT-xTB calculation took  $<2$  days whereas reference calculations needed several months to be completed. Note that with the most recent stda<sup>87</sup> implementation, the computation time could now be decreased to few hours. Figure 7 shows sTD-DFT-xTB frequency dispersion compares well to reference ONIOM ones.

A first application to compute second-order NLO responses with the sTD-DFT method was done by Seibert et al.<sup>30</sup> They investigated dynamic structural effects on the first hyperpolarizability of “flexible” tryptophan-rich peptides as

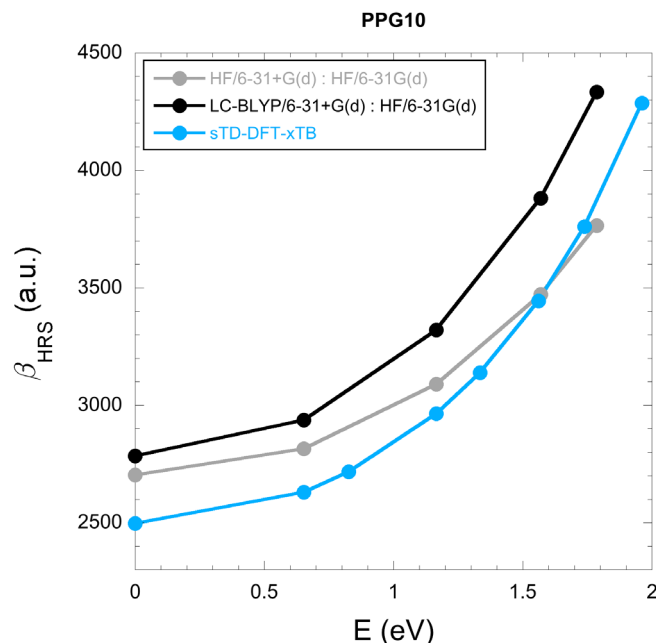


**FIGURE 7** Frequency dispersion of  $\beta_{\text{HRS}}$  for PPG10, calculated at the sTD-DFT-xTB level of theory and compared with ONIOM HF/6-31+G(d):HF/6-31G(d) and LC-BLYP/6-31+G(d):HF/6-31G(d) results.<sup>92,144</sup> Adapted with permission from de Wergifosse and Grimme.<sup>92</sup> Copyright 2018, AIP Publishing.

well as for gramicidin A. Conformer spaces were sampled for each peptide by the CREST<sup>145</sup> program and molecular dynamics (MD) simulations were done with the GFN2-xTB method.<sup>65</sup>  $\beta_{\text{HRS}}$  values were computed with the sTD-DFT-xTB method for which exchange and Coulomb parameters  $y_K$  and  $y_J$  (see Equations (35) and (34)) were fine-tuned to reproduce CCSD(T) reference calculations for tryptophan. For each conformer ensemble, Boltzmann-weighted  $\beta_{\text{HRS}}$  values were computed.  $\beta_{\text{HRS}}$  values were also averaged accounting for snapshots of MD simulations. These results were compared with standard TD-HF with and without implicit solvation as well as to experiment.

Structure–property relationships were first assessed for KWK, KWWK, KWWWK, and KWWKWWK (with W = tryptophan and K = lysine). While K side chain orientations have only a negligible impact on the SHG response, orientations among W units influence the  $\beta_{\text{HRS}}$  strongly. When indole units are parallel, dipolar  $\beta$  contributions add to each others, leading to enhanced SHG signals. Figure 8 present unit-sphere representations that map the  $\beta$ -tensor for two KWWK conformers. The conformer on the left-hand side presents two parallel tryptophan units and a clear dipolar character, confirmed by its depolarization ratio (DR). In contrast, when two indole moieties are anti-parallel, dipolar contributions of W units to the SHG signal cancel each other, leading to an octupolar character as shown on the right-hand side of Figure 8. This is confirmed by a typical DR value of 1.99 for an octupolar chromophore. Increasing the number of W units from KWK to KWWKWWK will not increase linearly the SHG response because it depends on orientations of W units. Sampling the conformational space or taking snapshots from MD simulations provided similar results. The ratio between both highest and lowest  $\beta_{\text{HRS}}$  values between conformers or snapshots can amount to a factor 2 to 6, depending on orientations of W units. They concluded from this that assessing dynamic structural effects are essential for determining the SHG response of these flexible systems.

Comparing sTD-DFT-xTB and TD-HF results accounting or not for implicit solvent effects to experiment<sup>146</sup> reveals the non-negligible impact of solvent effects to these systems. Regarding model peptides, both methods reproduce the experimental ordering, but only when accounting for solvent effects (see Figure 9).

Beaujean et al.<sup>27</sup> proposed a new all-atom quantum mechanics methodology to compute the SHG of fluorescent proteins (FPs). In this scheme, geometry optimizations are done at the ONIOM level using DFT ( $\omega$ B97X-D/6-31G\*) for the chromophore and its first shell of surrounding amino-acids (about 400 atoms) in the high layer. The remaining of the FP is treated at the GFN2-xTB/GBSA level in the low layer. The SHG of FPs are computed at sTD-DFT-xTB/GBSA(water) level of theory. The dt-sTD-DFT method mentioned in Section 2.3 was developed in this context to reduce the computational cost of sTD-DFT-xTB calculations. This methodology was tested on two

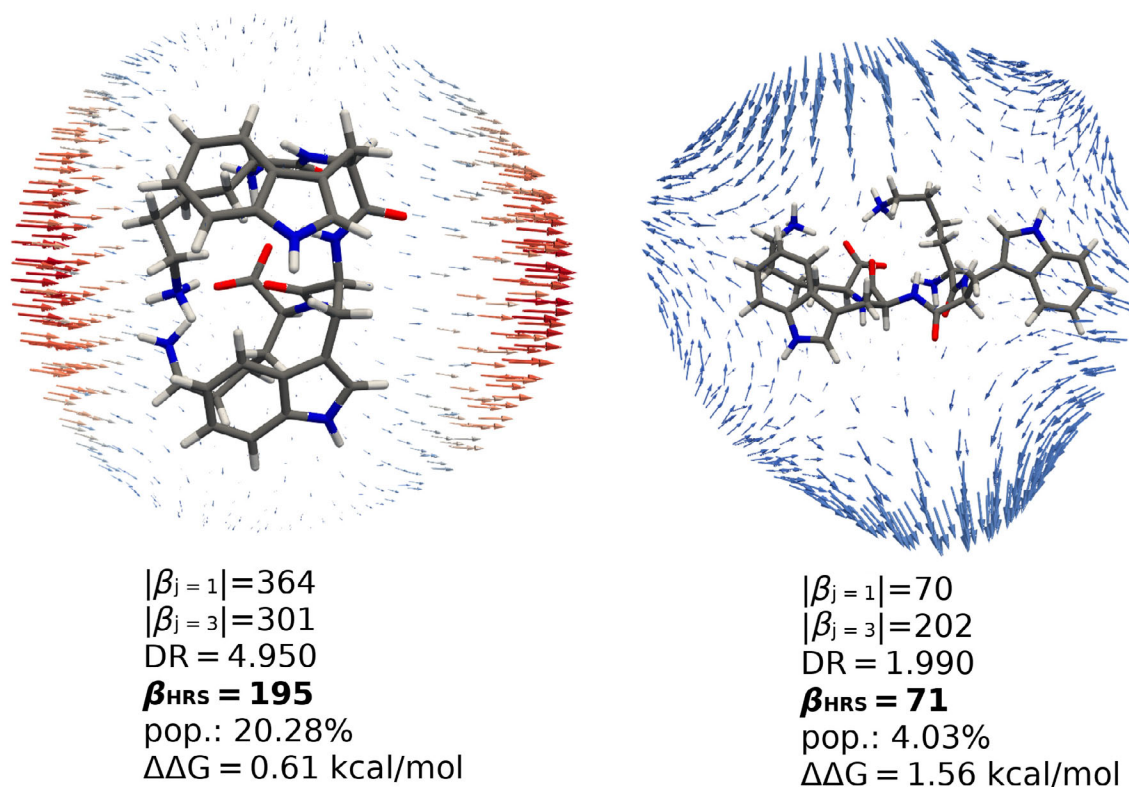


**FIGURE 8** Unit-sphere representation of two different conformers of the KWWK peptide. Left: Conformer 2 with parallel aligned tryptophan units. Right: Conformer 5 with anti-parallel tryptophan units. Vector fields are scaled differently for the sake of visibility.<sup>30</sup> Reprinted with permission from Seibert et al.<sup>30</sup> Copyright 2020, American Chemical Society.

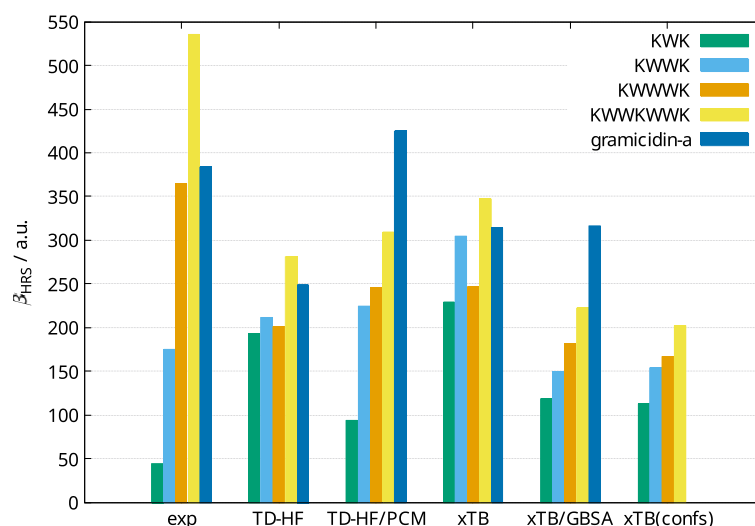


**FIGURE 9** Static first hyperpolarizabilities for KWK, KWWK, KWWWK, KWWKWWK, gramicidin A extrapolated from experiment and computed with TDHF/6-31+G(d), TDHF/6-31+G(d)/PCM, sTD-DFT-xTB, sTDDFT-xTB/GBSA, and Boltzmann weighted ensemble with sTD-DFT-xTB/GBSA.<sup>30</sup> Reprinted with permission from Seibert et al.<sup>30</sup> Copyright 2020, American Chemical Society.

FPs: iLOV ( $\approx 2000$  atoms, flavin mononucleotide chromophore) and the bacteriorhodopsin (bR,  $\approx 3850$  atoms, retinal Schiff base chromophore).

Optimized geometries show relatively small deviations with respect to experimental structures maintaining the  $\pi$ -conjugation of chromophores, thanks to the DFT inner layer. To fine-tune the sTD-DFT-xTB scheme, exchange  $y_K$



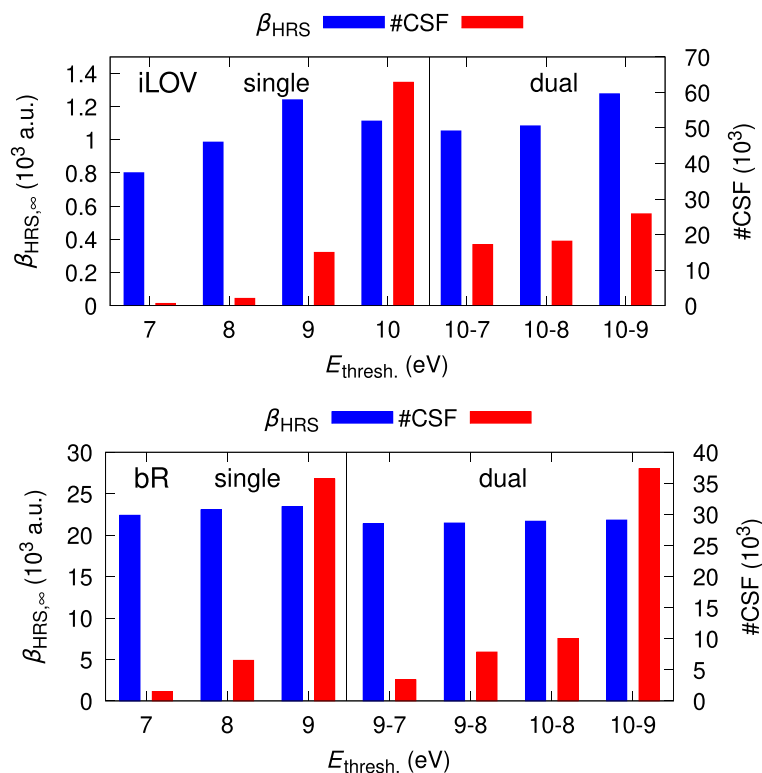


**FIGURE 10** Influence of  $E_{\text{thresh.}}$  on the static  $\beta_{\text{HRS}}$  of iLOV (top) and bR (bottom), as computed at the sTD-DFT-xTB level of theory (with  $y_f = 2.0$  and  $y_K = 0.15$ ) in water (GBSA), and corresponding numbers of CSFs. For the dual-threshold scheme, the first number indicates  $E_{\text{high}}$  and the second  $E_{\text{low}}$ .<sup>27</sup> Reprinted with permission from Beaujean et al.<sup>27</sup> Copyright 2021, American Chemical Society.

and Coulomb  $y_f$  parameters (Equations (34) and (35)) were optimized for chromophores to reproduce reference MP2 data.  $\beta_{\text{HRS}}$  dispersion curves for FPs were computed at the sTD-DFT-xTB/GBSA level of theory using both single and dual threshold schemes. Considering the dt-sTD-DFT, the high level part includes the chromophore only. Note that the scheme selected occupied MOs that have at least 10% of electron densities on the chromophore, meaning that they can extend beyond the high level part.

Using the single threshold scheme, static  $\beta_{\text{HRS}}$  values are improved when increasing the number of CSFs as shown in Figure 10. For bR, with  $E_{\text{thresh.}} = 7\text{ eV}$ ,  $\sim 1500$  CSFs are included in the sTD-DFT procedure, leading to a static  $\beta_{\text{HRS}}$  value already near the reference value ( $E_{\text{thresh.}} = 9\text{ eV}$ ,  $\sim 36,000$  CSFs). Note that the reference calculation took 74 h on a AMD Epyc CPU with 64 cores. The dt-sTD-DFT scheme converges faster. For bR, the static  $\beta_{\text{HRS}}$  value obtained with  $E_{\text{high}} = 9\text{ eV}$  and  $E_{\text{low}} = 7\text{ eV}$  is similar to the reference value but the calculation includes 10 times less CSFs and just took 5 hours to be computed. For FPs, this study advocated that at least  $E_{\text{high}}$  of 9 eV should be used for the sake of accuracy while  $E_{\text{low}}$  can be lowered by a few eV.

For bR, Figure 11 compares the sTD-DFT-xTB/GBSA  $\beta_{\text{HRS}}$  frequency dispersion to experiment from de Coene et al.<sup>147</sup> as well as to its extrapolation to the static limit using a simple vibronic model. Outside of the two-photon resonance area of the frequency dispersion curve, computed  $\beta_{\text{HRS}}$  values reproduce very well the experiment, demonstrating the robustness of our all-atom methodology to provide quantitative agreement with experiment. As expected, the quadratic response function diverges in resonance by design. Note that it was only possible to reproduce the two-photon resonance energy when including surrounding effects. This shows the importance to account for the whole protein into the quadratic response calculations.

Another application of the sTD-DFT method to evaluate the SHG of challenging systems was on self-assembled FONs consisting of dipolar  $\pi$ -conjugated push-pull chromophores with a strong electron-withdrawing group shown in Figure 12.<sup>28</sup> Lescos et al.<sup>28</sup> considered nanoparticles composed of 100 dyes and 46,850 water molecules that were self-aggregated during classical MD simulations of 250–300 ns at room temperature. The SHG of these FONs were evaluated in three ways: (i)  $\beta$  tensors were computed for each dyes at the TD-DFT M06-2X/6-311+G(d) level of theory and the first hyperpolarizability of the whole nanoparticle was obtained by tensor summation, (ii) the same procedure was

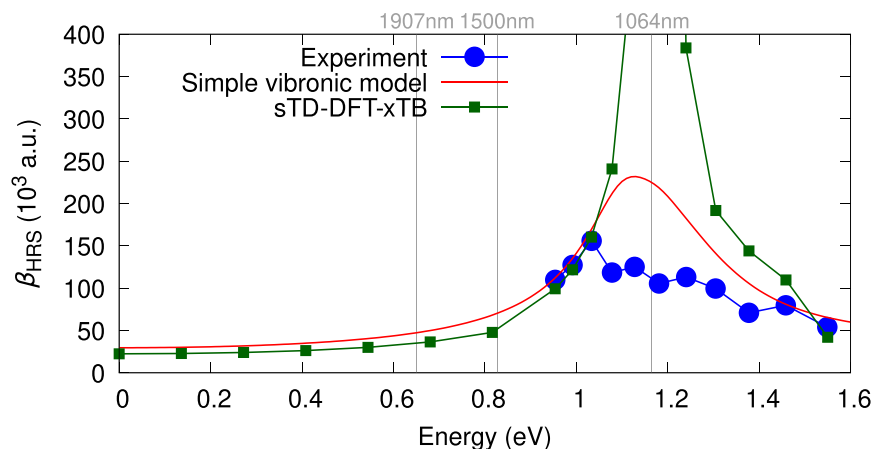


**FIGURE 11** Experimental versus calculated  $\beta_{\text{HRS}}$  frequency dispersion of bR. The experimental one<sup>147</sup> has been extrapolated (red curve) to the static limit by using a vibronic model. The calculations were carried out at the sTD-DFT-xTB level ( $y_J = 2.0$ ,  $y_K = 0.15$ , and  $E_{\text{thresh.}} = 9$  eV) in water (GBSA).<sup>27</sup> Reprinted with permission from Beaujean et al.<sup>27</sup> Copyright 2021, American Chemical Society.

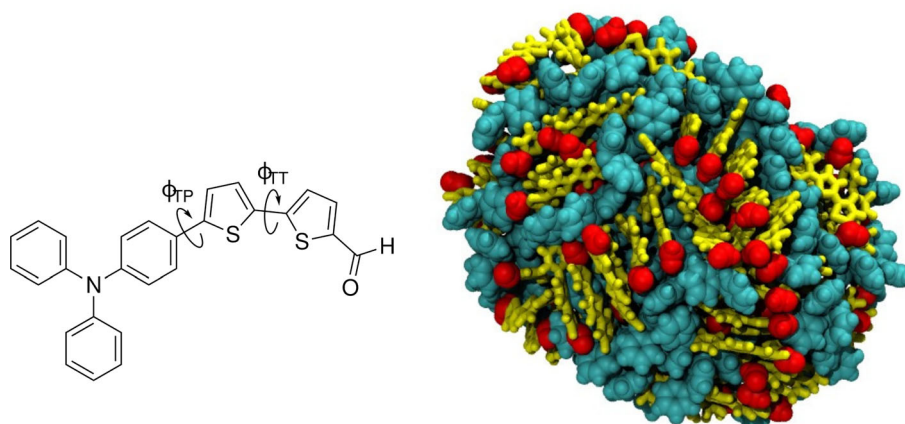


**FIGURE 12** Lewis structure (left) of the dye investigated by Lescos et al.<sup>28</sup> and dihedral angles. Example (right) of ellipsoidal nanoparticle composed of 100 aggregated dyes highlighting the orientation of formyl groups (in red) toward the outside, and the  $\pi$ -stacked domains (in yellow). Reprinted with permission from Lescos et al.<sup>28</sup> Copyright 2021, Royal Society of Chemistry.

applied but at the sTD-DFT-vTB level (diffuse functions were removed from the XBS) and, (iii) the entire nanoparticle was used for the sTD-DFT-vTB calculation. Note that exchange  $y_K$  and Coulomb  $y_J$  parameters used in the sTD-DFT-vTB procedure were fine-tuned to reproduce reference M06-2X/6-311G(d) calculations for the isolated chromophore as well as supramolecular clusters containing 12 dyes. No default parameters exist for the vTB flavor.

During the clustering procedure, most of hydrophobic triphenylamine groups stacked in parallel, creating sub-clusters containing up to 20 dyes. These sub-clusters cause the enhanced dipolar character of FONs. Antiparallel  $\pi$ -stacking was also observed. As it was shown for tryptophan-rich peptides<sup>30</sup> above, a correlation between  $\pi$ -stacking interactions, dipolar character, and enhanced  $\beta_{\text{HRS}}$  was enlightened. This relation depends on the nature of dyes involved. To analyze the impact of non-covalent interactions on the first hyperpolarizability of FONs, Lescos et al.<sup>28</sup> compared dynamic  $\beta_{\text{HRS}}$  sTD-DFT-vTB values computed using the tensor summation to sTD-DFT-vTB calculations considering the entire nanoparticle. sTD-DFT-vTB calculations on the entire system provide  $\beta_{\text{HRS}}$  values at 1064 nm enhanced in average by a factor  $\sim 3$  with respect to results obtained by tensor summation, in line with experimental findings. The one photon absorption spectrum for one representative nanoparticle was computed at the sTD-DFT-vTB level of theory. The computed spectral shape was consistent with measured FON suspensions in water, showing a broad main absorption band redshifted with respect to what it is observed for non-aggregated dyes in organic solvents. The experimentally observed absorption in the long-wavelength region (500–550 nm) is also observed. This is partly due to intermolecular charge-transfer excitations. This low energy band is responsible for the enhancement of the dynamic

$\beta_{\text{HRS}}$  at 1064 nm upon aggregation. In comparison to experiment, the computed  $\beta_{\text{NP}}/\beta_{\text{dye}}$  ratio is one order of magnitude too small. This was attributed to the small size of nanoparticles used for the calculations with respect to experimental ones (5 nm vs. 36 nm) as well as missing explicit interactions with the solvent.

### 3.2 | Two-photon absorption

In 1964, a pioneering study by Evleth and Peticolas<sup>148</sup> conducted theoretical calculations to evaluate the 2PA of pyrene and 3,4-benzopyrene (up to 32 atoms) using SCF-CI  $\pi$ -electron wave functions, based on the Pariser-Parr-Pople MO model<sup>35,149</sup> and the second-order time-dependent perturbation approach from Göppert-Mayer.<sup>1</sup> Calculated 2PA cross sections were found to be significantly higher with respect to experimental ones, but with correct trends, validating the underlying theory. To the best of our knowledge, only very few theoretical investigations on the 2PA of organic molecules using semi-empirical methods were performed at that time. This includes studies on vitamin A derivatives and other  $\pi$ -conjugated organic molecules<sup>150–153</sup> (<50 atoms). In 1979, Marchese et al.<sup>154</sup> employed the semi-empirical CNDO/S-CI method again coupled with the perturbation theory from Göppert-Mayer to investigate the 2PA properties of eight neutral molecules (<20 atoms): biphenyl, terphenyl, 2,2'-difluorobiphenyl, 2,2'-bipyridyl, phenanthrene, fluorene, carbazole, and dibenzofuran. The focus was on transition energies, symmetries, and relative 2PA cross-sections. Results showed reasonable agreements with respect to experiment.

More than 15 years later, in 1998, Brédas and coworkers<sup>155</sup> proposed design strategies for stilbene derivatives (up to 34 atoms) to enhance their 2PA cross sections. The 2PA cross-sections and transition energies were obtained at the INDO/MRD-CI (multi-reference double configuration interaction) level of theory using SOS expressions to compute 2PA strengths. Geometries were obtained with the AM1 method. Results showed significant increases in 2PA cross sections upon elongation of the conjugation path or enhanced symmetrical charge transfer between terminal and middle groups (i.e., stronger donor and acceptor groups). While the theoretical model showed good agreement with respect to experiment to reproduce excitation energy trends, computed excitation energies were systematically overestimated due to the over-correlation of the MRD-CI ground state. Nevertheless, experimental results supported by theoretical design strategies confirmed that longer  $\pi$ -conjugations and stronger acceptor and donor groups led to higher 2PA cross sections. In 2007, Brédas and coworkers<sup>156</sup> investigated the 2PA of a range of bis(acceptor)-substituted bis(dibutoxythienyl) ethene and bis(*N*-hexylpyrrolyl)ethene chromophores, each consisting of about 90 atoms, which was considered large at the time. As for the previous study, they<sup>156</sup> employed AM1 geometries and a modified ZINDO/MRD-CI for excited state calculations without considering solvent effects. Calculated 2PA cross sections were approximately half of experimental ones, but the theory successfully reproduced experimental spectral shapes and trends. Again, transition energies were overestimated due to the over-correlated MRD-CI ground state.

Nowadays, 2PA cross-sections are mainly computed using TD-DFT<sup>157–170</sup> or RI-CC2<sup>168,171–177</sup> methods limiting system sizes to a couple of hundreds of atoms. This limit could be extended by using INDO, ZINDO/S, or TD-DFTB2 semi-empirical methods. These methods are fast enough to be used for screening purposes, but their accuracy should be benchmarked carefully. Rossano-Tapia and Brown<sup>29</sup> showed in 2019 for a set of 22 FP chromophores that TD-DFTB2 2PA cross sections and excitation energies exhibit similar deficiencies as the “parent” GGA functional PBE. In particular, TD-DFTB2 underestimates excitation energies and transition dipole moments and overestimates differences between excited and ground state permanent dipole moments, leading to large errors in  $\sigma^{2PA}$ . Rossano-Tapia and Brown<sup>29</sup> concluded that TD-DFTB2 is not well-suited for evaluating  $\sigma^{2PA}$ . In 2014, Nayyar and Masunov<sup>178</sup> compared 2PA spectra obtained with PM6 and ZINDO/S methods to TD-DFT results and experimental data. The ZINDO/S method provides better  $\sigma^{2PA}$  than PM6, but both methods show larger errors than TD-DFT with respect to experiment. The same year, Silva et al.<sup>23</sup> explored the effect of explicit solvation on the 2PA spectrum of the fluorescein dianion (FSD). This study combines classical MD simulations for structure generation, with INDO/CIS and INDO/CISD calculations for excited states, and the SOS approach to compute 2PA cross-sections. A total of 250 snapshots were taken from a MD simulation. Their largest calculations encompassed a system of 176 atoms while they considered 150 excited states. They showed that the inclusion of doubly-excited configurations are important to describe the high-energy region of the 2PA spectrum. Solvent effects are mainly visible in the mid-energy region (300–400 nm), leading to different peak heights and an energy splitting of one 2PA band. Calculations are red-shifted with respect to experimental data. Accounting for the explicit surroundings improved overall the 2PA spectrum. Two SOS models were compared with compute 2PA cross-sections: the full expression (FE) and the resonant expression (RE) only considering resonant terms in the summation. Comparisons of SOS RE and FE approaches showed that

neglecting non-resonant terms only influences slightly the 2PA spectrum, with solvatochromic effects more distinct using the FE scheme.

Last year, de Wergifosse et al.<sup>94</sup> implemented the ultra-fast evaluation of 2PA cross-sections at the sTD-DFT level of theory in the stda program.<sup>87</sup> Three of their test cases considered large systems (Figure 13) to compare with experiment: (i) the eGFP,<sup>179</sup> (ii) a quadrupolar chromophore (**A**) and its branched version (**B**),<sup>180</sup> (iii) the flavin mono-nucleotide (FMN),<sup>172,181</sup> and the iLOV FP for which the FMN is the chromophore.

For eGFP, the structure of the chromophore and its first shell of surrounding residues including internal water molecules (359 atoms) was taken from Reference 139. Excitation energies and 2PA cross-sections were evaluated at the sTD-DFT-xTB level of theory with and without solvent effects, using GBSA as solvent model for water. Figure 14 compared computed 2PA spectra with respect to experiment. While no energy shifts were applied to calculated excitation energies, the agreement with respect to experiment is striking, especially when implicitly accounting for solvent effects.

This test was followed by a large organic, quadrupolar chromophore **A** and its branched version **B** that was measured experimentally by Katan et al.<sup>180</sup> Experimentally, **A** and **B** absorb around the same energy, but **B** exhibits a 3.2 times higher cross-section than **A** (see Figure 15). Quadrupolar molecules were optimized at the  $\omega$ B97X-D3/6-311G

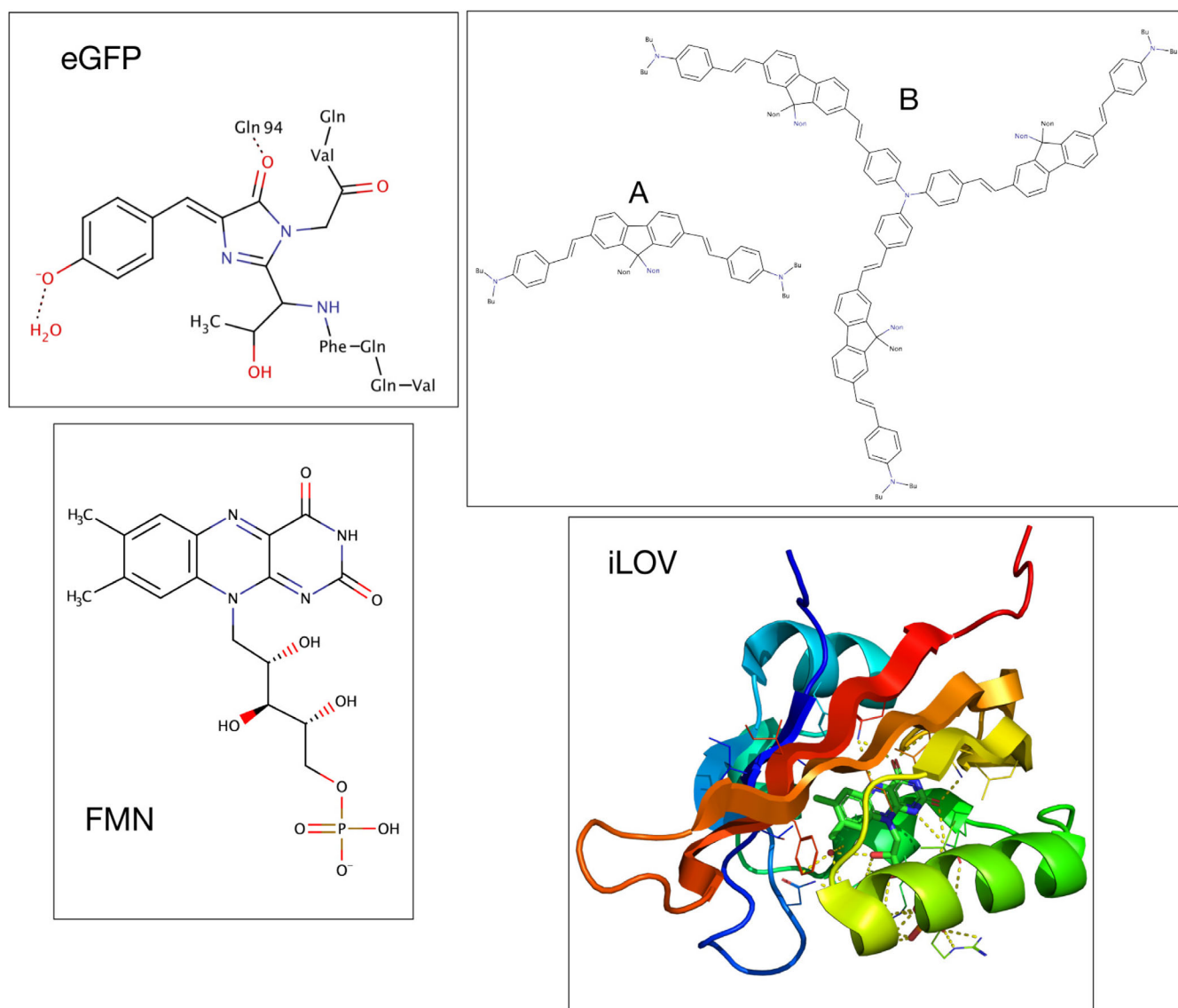


**FIGURE 13** Structure of the eGFP chromophore with its first shell of residues, the quadrupolar chromophore (**A**), its branched version (**B**), the flavin mono-nucleotide (FMN), and the iLOV protein. Adapted with permission from de Wergifosse et al.<sup>94</sup> Copyright 2022, American Chemical Society.

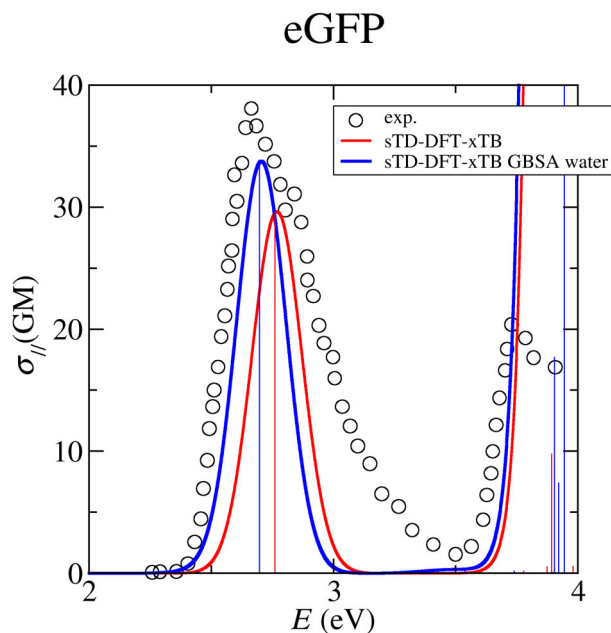


**FIGURE 14** Experimental 2PA spectrum measured by Drobizhev et al.<sup>179</sup> in comparison with the sTD-DFT-xTB computed for  $E_{\text{thresh.}} = 7$  eV,  $\Gamma = 0.1$  eV, and  $N = 2$  with and without solvent effects using GBSA model with water as solvent. Reprinted with permission from de Wergifosse et al.<sup>94</sup> Copyright 2022, American Chemical Society.

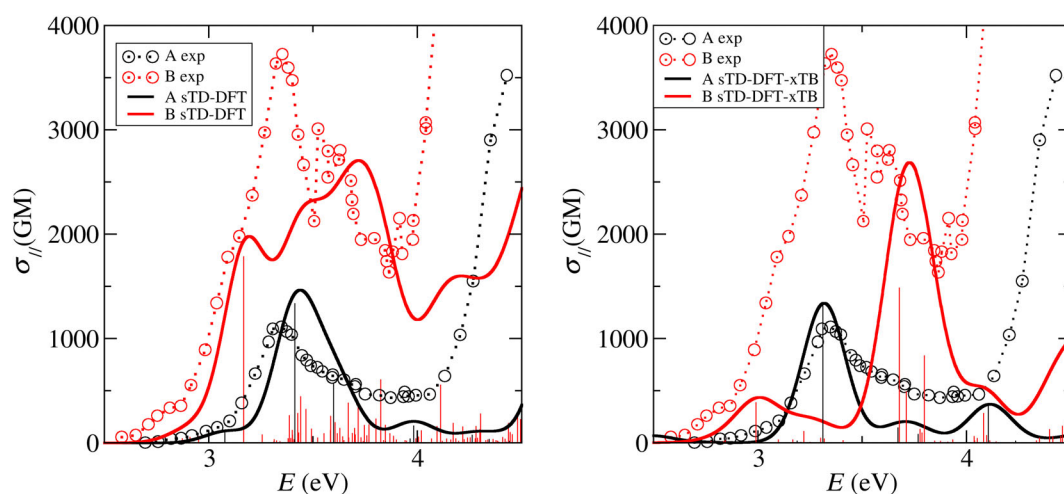


**FIGURE 15** Experimental 2PA spectra for the quadrupolar chromophore **A** and its branched version **B**<sup>180</sup> as well as theoretical spectra obtained at both sBHandHLYP/6-31+G(d) and sTD-DFT-xTB levels of theory considering  $N = 1$ ,  $\Gamma = 0.1$  eV,  $E_{\text{thresh.}} = 7$  eV, and systematic energy shifts of  $-0.65$  and  $-1.5$  eV, respectively for both methods. Reprinted with permission from de Wergifosse et al.<sup>94</sup> Copyright 2022, American Chemical Society.

(d) level of theory. Molecular orbitals and their energies were obtained with the xTB model as well as with the BHandHLYP functional using the 6-31+G(d) basis set. The sTD-DFT method was used to compute excitation energies and 2PA cross-sections. Both sBHandHLYP and sTD-DFT-xTB scheme reproduce well the experimental 2PA spectra of **A**. For the branched trimer **B**, a reasonable agreement with respect to experiment is reached with the sBHandHLYP method. However, the  $\sigma^{2PA}$  of the first intense transition is underestimated. Some of us<sup>94</sup> speculated that this discrepancy might be due to missing contributions from other conformers. The sTD-DFT-xTB method totally failed at reproducing the large first intense peak. Note that both theoretical spectra were shifted to account for missing effects.

Finally, the FMN chromophore was extracted from iLOV optimized structure from Reference 27 and its conformer ensemble was generated at 298.15 K with CREST<sup>145</sup> at the GFN2-xTB/GBSA(water) level of theory. Lower energy



conformers were optimized with the  $\omega$ B97X-D/6-31G(d)/IEFPCM(water) method. sTD-DFT-xTB 2PA spectrum for the lowest energy conformer as well as the Boltzmann weighted spectra were compared with experiment<sup>172,181</sup> (Figure 16). Accounting for the conformer ensemble broadens the lowest energy 2PA peak, but theoretical spectra remain similar. Comparing both computed 2PA spectra to experiment showed that the theory overestimates the energy difference between both 2PA main peaks by about  $\sim 0.5$  eV. This discrepancy is due to missing interactions with explicit water molecules as shown by List et al.<sup>172</sup> The optimized structure of iLOV was taken from the work of Beaujean et al.<sup>27</sup> mentioned in Section 3.1. The 2PA spectra for the full protein was computed at the sTD-DFT-xTB/GBSA(water) level of theory and compared with experiment<sup>181</sup> (Figure 16). The first experimental peak around 2.9 eV is remarkably well reproduced by the sTD-DFT-xTB scheme. The second peak is blue-shifted.

### 3.3 | Excited-state absorption

To evaluate ESA, the double residue of the first hyperpolarizability (Equation (49))<sup>73</sup> give direct access to state-to-state transition dipole moments.<sup>24,182–184</sup> ESA can also be obtained from real-time methods. There, transition dipole moments are evaluated from the time fluctuation of the density matrix.<sup>184,185</sup> Comparable results are obtained with both approaches.<sup>186</sup> Note that generally the Tamm–Dancoff approximation is employed, but it does not affect much computed ESA spectra.<sup>187</sup> Early implementations of excited-to-excited transition dipole moments were available in ZINDO/S, as these quantities are required for the SOS evaluation of  $\beta$ ,  $\gamma$ , and 2PA.<sup>188,189</sup> However, only few examples focused on the ESA.<sup>190</sup> More recently, de Wergifosse and Grimme<sup>24</sup> provided implementations in the stda program<sup>87</sup> at both sTDA and sTD-DFT levels. Another recent implementation at the time-independent excited-state density-functional tight-binding ( $\Delta$ DFTB) level<sup>191</sup> also exists, but systems studied by Deshayé et al.<sup>191</sup> are relatively small with respect to the subject of this review.

Among the systems studied in the sTDA/sTD-DFT ESA seminal paper,<sup>24</sup> the ESA of the first and second singlet excited states for a fullerene derivative (*N*-methylfulleropyrrolidine) were evaluated at the sTD-DFT/ $\omega$ B97X-D3/6-311+G(d,p) level. Its geometry was optimized with PBE0/6-311G(d) method. These results were compared with experimental transient ESA spectra from Reference 192 (Figure 17, left panel). Guldi and Prato<sup>192</sup> wrongly attributed these spectra to the first singlet and first triplet excited states while sTD-DFT/ $\omega$ B97X-D3 results showed undoubtedly that these spectra correspond to the two first singlet excited states. The largest system studied by de Wergifosse and

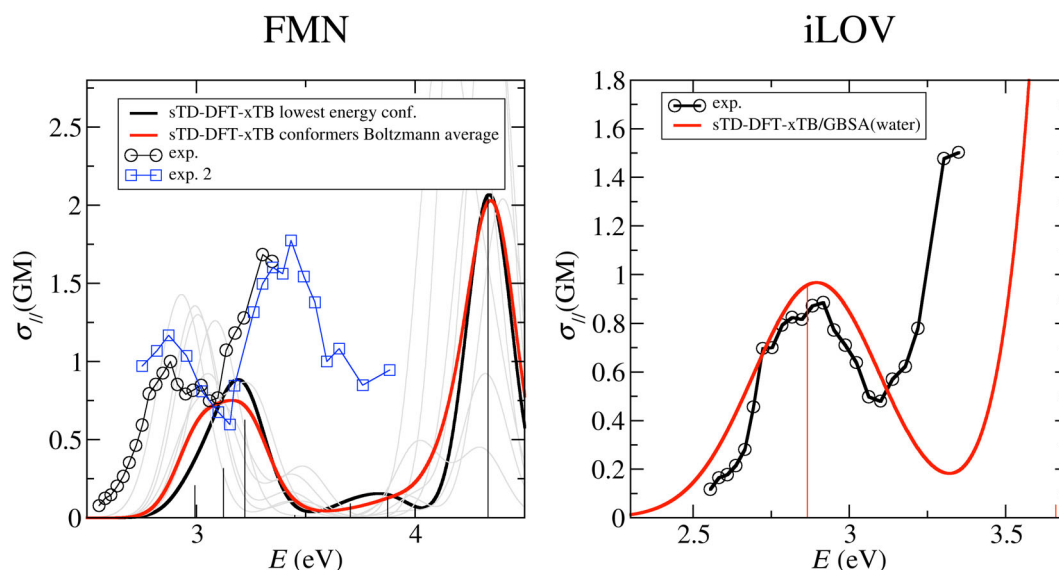


**FIGURE 16** Experimental 2PA spectra of the FMN in water solution (left panel) from Homans et al.<sup>181</sup> and List et al.<sup>172</sup> as well as theoretical spectra obtained at the sTD-DFT-xTB levels of theory considering  $N = 1$ ,  $\Gamma = 0.1$  eV, and  $E_{\text{thresh.}} = 7$  eV for the 8 lowest energy conformers as well as the Boltzmann average for these conformers at 298.15 K. Experimental 2PA spectrum of iLOV (right panel) from Homans et al.<sup>181</sup> as well as the theoretical spectrum obtained at the sTD-DFT-xTB/GBSA(water) level of theory considering  $N = 1$ ,  $E_{\text{thresh.}} = 7$  eV, and  $\Gamma = 0.2$  eV. Reprinted with permission from de Wergifosse et al.<sup>94</sup> Copyright 2022, American Chemical Society.



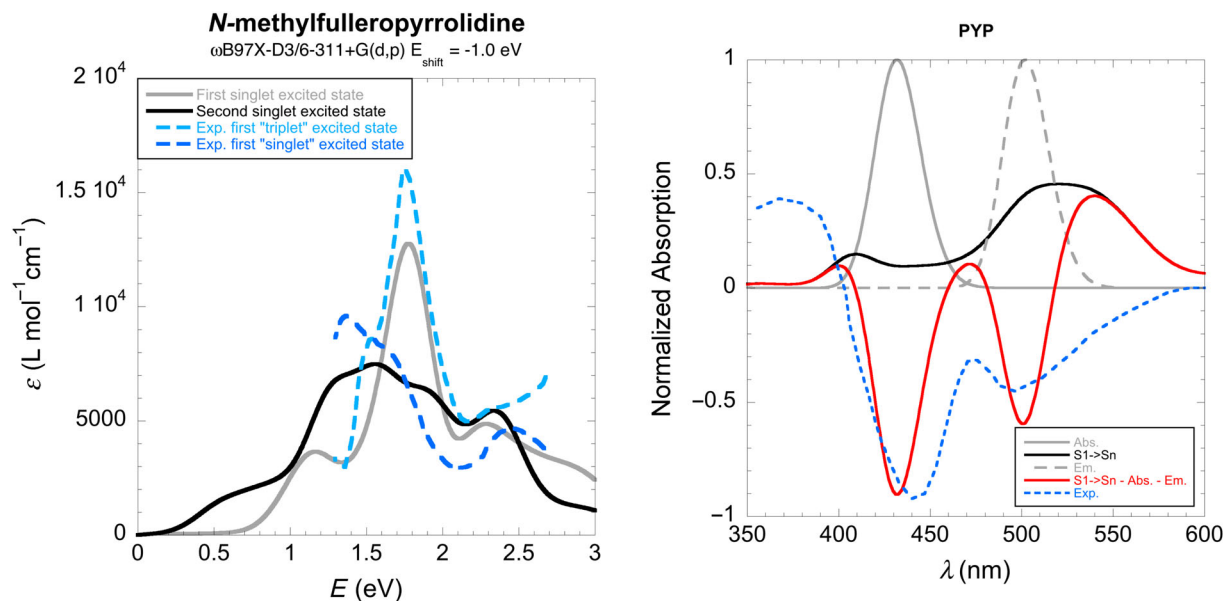


**FIGURE 17** Transient ESA spectra of *N*-methylfulleropyrrolidine<sup>192</sup> (left panel) in toluene following a picosecond flash photolysis at 355 nm, attributed to the first singlet excited state and the first triplet excited state compared with sTD-DFT/ $\omega$ B97X-D3/6-311+G(d,p) calculations for the first and second singlet excited-state absorption spectra shifted by  $-1.0$  eV. Transient absorption of PYP<sup>194</sup> (right panel) in 10 mM Tris-HCl buffer solution at pH 8.1, 1.5 ps after a 370 nm actinic excitation, compared with sTDA-xTB first singlet excitation, absorption, “fake” stimulated emission, and the simulated transient spectra. Reprinted with permission from de Wergifosse and Grimme.<sup>24</sup> Copyright 2019, AIP Publishing.

Grimme<sup>24</sup> was the photoactive yellow protein (PYP), a small protein composed of 1931 atoms. PYP optimized geometry was taken from Seibert et al.<sup>193</sup> The ESA of the first singlet excited state of PYP was computed at the sTDA-xTB level. From the ESA, one of us subtracted ground state absorption as well as the “fake” stimulated emission (ground state absorption shifted by 70 nm) to compare to the experimental transient absorption recorded by Changenet-Barret et al.<sup>194</sup> An excellent agreement with respect to experiment was obtained reproducing main features of the experimental transient absorption.

### 3.4 | Second hyperpolarizability

The molecular second hyperpolarizability is generally less studied than  $\beta$  because it is experimentally challenging to measure. Implementations to evaluate  $\gamma$  in QC codes are also sparse. In 1967,  $\gamma$  was computed using the FF method for small systems including  $\pi$ -conjugated hydrocarbons, polyenes, cyanine, merocyanine, and pyridiniumbetain dyes (<30 atoms).<sup>104</sup> Fifteen years later, Papadopoulos et al.<sup>131,132</sup> studied the THG of aromatic systems and polyenes theoretically with the FF approach and a CNDO model, yielding reasonable comparisons to experimental data. In 1990, the MOPAC program was able to evaluate  $\gamma$  using a FF implementation.<sup>121</sup> This led to several studies<sup>106,121,195</sup> with systems including <50 atoms. In general, those results compared reasonably well with respect to experiment (e.g.,  $R^2 > 0.9$  of correlation with respect to experiment for stibazonium salts<sup>195</sup>).

The SOS approach was also used to evaluate  $\gamma$ . Tian<sup>129</sup> computed  $\gamma$  of  $C_{60}$  and  $C_{240}$  using CIS excited states for the SOS scheme at the ZINDO level of theory. The predicted  $\gamma$  of  $C_{60}$  was in good agreement with experiment. The second hyperpolarizability of  $C_{240}$  was estimated to be 30 times larger than the one of  $C_{60}$ . In 2020, Tian et al.<sup>196</sup> extended this study to fullerene anions with three layers ( $C_{60}@C_{240}@C_{540}$ ), for a total of 840 atoms.

Analytical calculations of  $\gamma$  imply the implementation of cubic response functions. In 1990, Waite and Papadopoulos<sup>109</sup> computed  $\gamma$  analytically using a CNDO Hamiltonian to study the impact of hydrogen bonds on the response of hydrogen fluoride multimers, up to 8 molecules. Later on, Malagoli and Thiel<sup>197</sup> studied the frequency-dependent  $\gamma$  response of aromatic (hetero)cycles as well as polymers (< 50 atoms) with a MNDO/d Hamiltonian, providing acceptable comparisons to experiment. Different semi-empirical methods (including MNDO, AM1, PM3, and

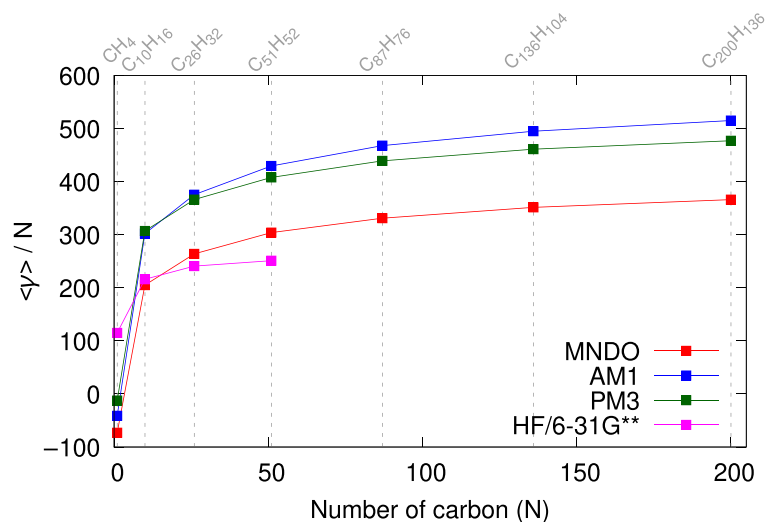


**FIGURE 18** Mean static second hyperpolarizability [ $\langle\gamma\rangle = \frac{1}{5}(\gamma_{xxxx} + \gamma_{yyyy} + \gamma_{zzzz} + 2\{\gamma_{xxyy} + \gamma_{xxzz} + \gamma_{yyzz}\})$ , in a.u.] per atom of carbon ( $N$ ) versus the number of atom in the cluster, as computed by semi-empirical methods and HF.<sup>200</sup> Adapted with permission from Bishop and Gu.<sup>200</sup> Copyright 2000, Elsevier Science B.V.A.

PM6, among others) using a TD-HF cubic response were later assessed by Avci<sup>198,199</sup> on donor-acceptor chromophores, advocating the use of PM6 or AM1 over MNDO.

In 2000, Bishop and Gu<sup>200</sup> studied  $\gamma$  for diamond models from  $\text{CH}_4$  to  $\text{C}_{200}\text{H}_{136}$ . Second hyperpolarizabilities were determined by FF differentiation of  $\beta$ , which were estimated by a coupled-perturbed approach using semi-empirical Hamiltonians. Results reproduced in Figure 18 show that AM1, and PM3 methods predict larger  $\langle\gamma\rangle$  values than TD-HF, while MNDO ones are similar. To extrapolate the static  $\gamma$  value of bare diamond, they used a least square fit ( $\langle\gamma\rangle = n_C \langle\gamma\rangle_C + n_H \langle\gamma\rangle_H$ , where  $n_C$  and  $n_H$  are the number of carbon and hydrogen in each cluster, respectively), which led to an estimate of  $\langle\gamma\rangle_C$ , the contribution of carbon atoms to the second hyperpolarizability. They also provided an estimate of  $\chi^{(3)}$  for diamond ( $\chi^{(3)} = \frac{N}{V} \langle\gamma\rangle_C = 2.68 \times 10^{-14}$  esu, where  $N$  and  $V$  are the number of atom and the volume of a unit cell of diamond). The comparison with the experimental value of  $\chi^{(3)} \approx 4.92 \times 10^{-14}$  indicates that semi-empirical methods and TD-HF underestimate the  $\gamma$  of diamond.

In 2017, the interest in the molecular second hyperpolarizability was reignited by the measurement of third harmonic scattering responses by two different groups.<sup>201,202</sup> Materials with large  $\chi^{(3)}$  are of great interest in photonics, but optical losses generally due to two-photon absorption should be minimized.<sup>21</sup> The help from theory for the design of new materials with large  $\gamma$  and minimal  $\sigma^{2PA}$  at the wavelength of interest is of the outmost importance. For this purpose, the implementation of the evaluation of  $\gamma$  at (X)STD-DFT levels of theory will be soon started in de Wergifosse's research group.

## 4 | CONCLUSIONS

This review presented developments and applications of modern sQC methods to compute non-linear optical properties of large systems as well as an historical overview of early semi-empirical schemes for this purpose. A particular focus was put on the sTD-DFT approach.<sup>22,87,89</sup> In 2018, this method emerged as an excellent alternative to evaluate NLO properties<sup>92</sup> for large systems. The evaluation of any response property is a two-step procedure that includes the calculation of the ground state, either with wave function theory or with density functional theory based methods, and consequently, the computation of response properties. As so, in the theory part of this review, we briefly addressed different methods as HF, DFT, and especially their semi-empirical counterparts to obtain ground states of large systems. This included DFTB variants: the successful xTB family of methods<sup>64</sup> including the GFN2-xTB<sup>65</sup> scheme to obtain ground state geometries as well as the xTB part of sTDA/sTD-DFT-xTB approaches<sup>61</sup> to determine ground state molecular orbitals and their energies. To compute NLO response properties, we succinctly reviewed standard procedures including FF, SOS, and TD-DFT methods. Then, a global view of sTDA/sTD-DFT methods<sup>22,87,89</sup> was given including their approximations and implementations to compute NLO properties such as the first hyperpolarizability,<sup>92</sup> excited state

absorption,<sup>24</sup> and two-photon absorption.<sup>94</sup> Details about the dt-sTD-DFT method<sup>27</sup> was given, a method specially designed to treat large systems with a central chromophore. The XsTD-DFT method was also introduced and will be soon more detailed in another publication. Because the XsTD-DFT scheme is not parameter dependent anymore, the distinction between semi-empirical methods and simplified ones is clearer.

The discussion part is divided in subsections for each NLO property of interest: the first hyperpolarizability, 2PA, ESA, and the second hyperpolarizability. Regarding the first hyperpolarizability, because its measurement can be easily implemented, most of past researches focused on this property. The simple FF approach was the first method used to compute the static first hyperpolarizability.<sup>104</sup> The SOS approach was the alternative route used at the time to compute static and dynamic first hyperpolarizabilities. We showed in this review how both techniques, along with Hückel or INDO Hamiltonian, were frequently applied for increasing system sizes in the late 20th century.<sup>108,110,118,119</sup> Coupled-perturbed methods emerged in the 1980s and 1990s as an alternative way to compute static first hyperpolarizabilities.<sup>130–132,135,136</sup> In the early 21st century, semi-empirical methods were mostly replaced by their full QM counterparts because of the improved computational power. Still nowadays, large systems containing up to several thousands of atoms such as FPs or FONs are out of the scope of standard time-dependent methods. This context motivates the extension of the sTD-DFT scheme to the evaluation of second-order response properties,<sup>92</sup> reigniting the interest for semi-empirical schemes to compute NLO properties. This review gave an overview of the first applications of the sTD-DFT method to compute the first hyperpolarizability of large ensembles of configurations for tryptophan-rich peptides and the gramicidin A<sup>30</sup> as well as ultra-large systems, including FONs<sup>28</sup> and FPs.<sup>27,92</sup> Thanks to the sTD-DFT implementation, first hyperpolarizabilities of such large systems can now easily be computed within hours to a few days while including effects of explicit surroundings. Simplified methods are a real asset to evaluate first hyperpolarizabilities especially with the current sTD-DFT-xTB approach that can deal with very large systems such as FPs and FONs. The sTD-DFT-xTB method enables to correctly reproduce the impact on  $\beta$  of structural dynamic effects, surroundings, and clustering in reasonable amount of time while keeping a decent accuracy. Seibert<sup>30</sup> shows that sampling the conformational space can have a large influence on second-order NLO properties especially for very flexible molecules such as peptides. It is also necessary to find the lowest energy conformer. Beaujean et al.<sup>27</sup> proposed the first all-atom QC methodology to compute the first hyperpolarizability of a system as large as a FP. They showed that surrounding effects need to be included to compute the frequency dispersion curve of bR to match experimental data. The dt-sTD-DFT scheme was proposed by Beaujean et al.<sup>27</sup> to decrease the computational cost of sTD-DFT calculations that include explicit environment effects. Finally, Lescos et al.<sup>28</sup> enlightened the origin of the large  $\beta$  enhancement of FONs thanks to the sTD-DFT-vTB scheme, showing that the aggregation process introduces lower energy excited states that are in two-photon resonance at the wavelength of the experiment.

Regarding 2PA, to the best of our knowledge, the first theoretical study was pioneered by Evleth and Peticolas<sup>148</sup> already in 1964 and followed by a few other studies.<sup>150–154</sup> In the late 1990s and at the start of the 21st century, using the SOS approach with the INDO/MRD-CI method to compute 2PA cross-section, Brédas and coworkers<sup>155,156</sup> proposed design strategies for bis(styryl)benzene derivatives as well as bis(acceptor)-substituted bis(dibutoxythienyl)ethene and bis(N-hexylpyrrolyl)ethene chromophores. After reviewing these works, recent studies using TD-DFTB2,<sup>29</sup> PM6, ZINDO/S,<sup>178</sup> INDO/CIS, and INDO/CISD<sup>23</sup> methods were presented. As the main subject of this review, we discussed in details the ultra-fast evaluation of 2PA cross-sections at the sTD-DFT level of theory<sup>94</sup> with three of its test cases: the eGFP, a quadrupolar chromophore and its branched version, as well as the FMN and iLOV. For eGFP, with a model including the chromophore and its first shell of surrounding residues, a striking agreement was obtained to reproduce the experimental 2PA spectrum at the sTD-DFT-xTB level of theory. Another FP called iLOV was also characterized at this level but including the entire protein into the calculation. Here again a striking agreement with respect to experiment was obtained while no energy shifts were applied. This result extended the all-atom QC methodology to the evaluation of 2PA cross-sections for systems as large as FPs.

Regarding ESA, to the best of our knowledge, only few studies focused on this property using semi-empirical methods.<sup>190</sup> In 2019,<sup>24</sup> the evaluation of ESA at the sTDA and sTD-DFT levels of theory was implemented in the stda program.<sup>87</sup> In this study, de Wergifosse and Grimme<sup>24</sup> interpreted the transient absorption of PYP with the help of a sTDA-xTB calculation for the ESA of the first singlet excited state showing the suitability of this method to treat large systems.

Finally, as it is not yet possible to evaluate the second hyperpolarizability with modern simplified methods, we only focused on studies involving the evaluation of  $\gamma$  using semi-empirical methods. Note that the second hyperpolarizability is usually less studied than  $\beta$  due to more challenging experimental requirements. Using FF methods, in the late 1960s,  $\pi$ -conjugated compounds were studied by Schweig.<sup>104</sup> This was followed by a few studies using the FF

approach.<sup>106,121,131,132,195</sup> More recently, the SOS approach was also used to evaluate  $\gamma$  at the ZINDO level of theory.<sup>129,196</sup> These studies included large fullerene onions containing up to 840 atoms. Using cubic response functions, a few studies appeared in the 1990s using CNDO and MNDO/d Hamiltonians.<sup>109,197</sup> Benchmark studies on donor-acceptor chromophores of semi-empirical methods with respect to TD-HF were provided by Avci.<sup>198,199</sup> One noteworthy study by Bishop and Gu<sup>200</sup> studied the second hyperpolarizability of diamond using AM1 and PM3 methods. In 2017, the interest in  $\gamma$  was reignited by measurements of the third harmonic scattering response.<sup>201,202</sup> For applications in photonics, materials with large  $\gamma$  and small 2PA cross-sections at the wavelength of interest are of the outmost importance. Soon, the implementation of  $\gamma$  at the sTD-DFT and XsTD-DFT levels of theory will start in de Wergifosse's research group.

A recent perspective article<sup>22</sup> reviewed method developments we planned for the future of sQC methods. Among them, the XsTD-DFT method was the solution we found to improve the global accuracy of the sTD-DFT scheme providing better first hyperpolarizability frequency dispersions while removing its semi-empiricism. For strongly correlated systems, while the spin-flip sTD-DFT (SF-sTD-DFT) method<sup>203</sup> already exists, we plan to implement other flavors such as a computationally efficient double hybrid version<sup>204,205</sup> of (X)sTD-DFT methods, simplified versions of spin-adapted (SA-)SF-TD-DFT<sup>206</sup> and mixed-reference (MR-)SF-TD-DFT<sup>207</sup> methods, or more ambitious method developments. We also suggested the reintroduction of an approximated exchange-correlation kernel as for DFTB methods.<sup>208</sup> Solvent implicit nonequilibrium effects should be introduced in the sda program.<sup>87</sup> The gradient and the Hessian is now being implemented for XsTD-DFT/XsTDA and sTD-DFT/sTDA methods. In addition, in terms of new developments for the evaluation of NLO properties of large systems, damped linear and nonlinear responses<sup>209–211</sup> in both sTD-DFT and XsTD-DFT frameworks will be implemented to cure for the divergent nature of response functions. Figure 11 illustrates the divergence of the sTD-DFT-xTB response function at the resonance with an excited state in comparison to experimental  $\beta_{\text{HRS}}$  spectrum for the bacteriorhodopsin.<sup>27</sup> This unphysical behavior is linked to infinite excited state lifetimes accounted for in response theory that can be solved using damped response theory. These new implementations will be extended to the evaluation of the third harmonic generation. For the moment, the xTB scheme is not working with the XsTD-DFT method precluding its use to treat large systems. The xTB scheme needs to be specifically optimized for this method. Furthermore, properties involving the magnetic moment operator will be explored, an area that remains untouched by most sQC implementations. The evaluation of magneto-optical properties such as the Faraday effect,<sup>212</sup> HRS optical activity, ...<sup>213</sup> will be implemented.

As demonstrated throughout this review, combining DFT or xTB ground states with the sTD-DFT method to compute NLO response properties allows the treatment of systems up to several thousand atoms or of large numbers of configurations. Consequently, computer-aided design of new (bio-)molecules with improved NLO properties, the fast screening of many molecules for NLO applications, and evaluating NLO properties of conformer/rotamer ensembles are now possible thanks to sQC methods. Currently, two of us are working on the impact of explicit surroundings on 2PA and the extension of the dt-sTD-DFT method to this property. This study includes the dynamical impact of including explicit solvent molecules on the 2PA response of the FMN.<sup>23,172</sup> The work on  $\beta$  and 2PA of FPs is currently extended to new types of FPs as well as to co-crystals where we aim at providing new design guidelines for enlarging  $\sigma_{2PA}$  via changes in the intermolecular architecture. The  $\gamma$  of these systems will be characterized as soon as the implementation will be available. This will allow to extend our all-atom QC methodology to the evaluation of  $\gamma$  of large systems. The work on the first hyperpolarizability of aggregates of dyes is also continuing. Other applications are envisioned for the future such as receptors in membranes, polymers, carbon dots, and so on.

## AUTHOR CONTRIBUTIONS

**Sarah Löffelsender:** Writing – original draft (equal); writing – review and editing (equal). **Pierre Beaujean:** Writing – original draft (equal); writing – review and editing (equal). **Marc de Wergifosse:** Conceptualization (lead); supervision (lead); writing – original draft (equal); writing – review and editing (equal).

## ACKNOWLEDGMENTS

Marc de Wergifosse thanks warmly Prof. Stefan Grimme for his trust in his work and the freedom he gave him when he was a postdoc, resulting to most of recent sQC method developments illustrated in this review. The authors thank Prof. Anna Krylov for the invitation to write this review.

## CONFLICT OF INTEREST STATEMENT

The authors declare no conflicts of interest.

## DATA AVAILABILITY STATEMENT

Data sharing is not applicable to this article as no new data were created or analyzed in this study.

## ORCID

Sarah Löffelsender  <https://orcid.org/0000-0003-3146-7810>

Pierre Beaujean  <https://orcid.org/0000-0003-3723-3257>

Marc de Wergifosse  <https://orcid.org/0000-0002-9564-7303>

## RELATED WIREs ARTICLES

[Extended tight-binding quantum chemistry methods](#)

## REFERENCES

1. Göppert-Mayer M. Über Elementarakte mit zwei Quantensprüngen. *Ann Phys (Berl)*. 1931;401:273–94. <https://doi.org/10.1002/andp.19314010303>
2. Maiman T. Stimulated emission of radiation in ruby. *Nature*. 1960;187:493–4.
3. Kaiser W, Garrett CGB. Two-photon excitation in  $\text{CaF}_2:\text{Eu}^{2+}$ . *Phys Rev Lett*. 1961;7:229–31. <https://doi.org/10.1103/PhysRevLett.7.229>
4. Franken PA, Hill AE, Peters CW, Weinreich G. Generation of optical harmonics. *Phys Rev Lett*. 1961;7:118–9. <https://doi.org/10.1103/PhysRevLett.7.118>
5. Terhune RW, Maker PD, Savage CM. Optical harmonic generation in calcite. *Phys Rev Lett*. 1962;8:404–6. <https://doi.org/10.1103/PhysRevLett.8.404>
6. Torres-Torres C, García-Beltrán G. Methods for measuring nonlinear optical properties. In: Torres-Torres C, García-Beltrán G, editors. *Optical nonlinearities in nanostructured systems*. Basel: Springer; 2022. p. 1–32.
7. Boyd RW. *Nonlinear optics*. 3rd ed. Amsterdam, Boston: Academic Press; 2008.
8. Verbiest T, Clays K, Rodriguez V. *Second-order nonlinear optical characterization techniques: an Introduction*. Florida: Taylor & Francis; 2009.
9. Raymo FM. Digital processing and communication with molecular switches. *Adv Mater*. 2002;14:401–14. [https://doi.org/10.1002/1521-4095\(20020318\)14:6<401::AID-ADMA401>3.0.CO;2-F](https://doi.org/10.1002/1521-4095(20020318)14:6<401::AID-ADMA401>3.0.CO;2-F)
10. Ironside CN. Nonlinear optical devices. In: Munn RW, Ironside CN, editors. *Principles and applications of nonlinear optical materials*. Dordrecht, Netherlands: Springer; 1993. p. 20–34.
11. Campagnola PJ, Wei M, Lewis A, Loew LM. High-resolution nonlinear optical imaging of live cells by second harmonic generation. *Biophys J*. 1999;77:3341–9. [https://doi.org/10.1016/S0006-3495\(99\)77165-1](https://doi.org/10.1016/S0006-3495(99)77165-1)
12. Campagnola PJ, Loew LM. Second-harmonic imaging microscopy for visualizing biomolecular arrays in cells, tissues and organisms. *Nat Biotechnol*. 2003;21:1356–60. <https://doi.org/10.1038/nbt894>
13. Campagnola P. Second harmonic generation imaging microscopy: applications to diseases diagnostics. *Anal Chem*. 2011;83:3224–31. <https://doi.org/10.1021/ac1032325>
14. Gu B, Zhao C, Baev A, Yong KT, Wen S, Prasad PN. Molecular nonlinear optics: recent advances and applications. *Adv Opt Photon*. 2016;8:328–69. <https://doi.org/10.1364/AOP.8.000328>
15. Karna SP, Dupuis M. Frequency dependent nonlinear optical properties of molecules: formulation and implementation in the HONDO program. *J Comput Chem*. 1991;12:487–504. <https://doi.org/10.1002/jcc.540120409>
16. Runge E, Gross EKH. Density-functional theory for time-dependent systems. *Phys Rev Lett*. 1984;52:997–1000. <https://doi.org/10.1103/PhysRevLett.52.997>
17. Christiansen O, Jørgensen P, Hättig C. Response functions from Fourier component variational perturbation theory applied to a time-averaged quasienergy. *Int J Quant Chem*. 1998;68:1–52.
18. Comeau DC, Bartlett RJ. The equation-of-motion coupled-cluster method. Applications to open- and closed-shell reference states. *Chem Phys Lett*. 1993;207:414–23. [https://doi.org/10.1016/0009-2614\(93\)89023-B](https://doi.org/10.1016/0009-2614(93)89023-B)
19. Norman P. A perspective on nonresonant and resonant electronic response theory for time-dependent molecular properties. *Phys Chem Chem Phys*. 2011;13:20519–35. <https://doi.org/10.1039/c1cp21951k>
20. Kanis DR, Ratner MA, Marks TJ. Design and construction of molecular assemblies with large second-order optical nonlinearities. Quantum chemical aspects. *Chem Rev*. 1994;94:195–242. <https://doi.org/10.1021/cr00025a007>
21. Bredas JL, Adant C, Tackx P, Persoons A, Pierce BM. Third-order nonlinear optical response in organic materials: theoretical and experimental aspects. *Chem Rev*. 1994;94:243–78. <https://doi.org/10.1021/cr00025a008>
22. de Wergifosse M, Grimme S. Perspective on simplified quantum chemistry methods for excited states and response properties. *J Phys Chem A*. 2021;125:3841–51. <https://doi.org/10.1021/acs.jpca.1c02362>
23. Silva DL, Barreto RC, Lacerda EG, Coutinho K, Canuto S. One- and two-photon absorption of fluorescein dianion in water: a study using S-QM/MM methodology and ZINDO method. *Spectrochim Acta A*. 2014;119:63–75. <https://doi.org/10.1016/j.saa.2013.04.035>
24. de Wergifosse M, Grimme S. Nonlinear-response properties in a simplified time-dependent density functional theory (sTD-DFT) framework: evaluation of excited-state absorption spectra. *J Chem Phys*. 2019;150:094112. <https://doi.org/10.1063/1.5080199>



25. Nénon S, Champagne B. SCC-DFTB calculation of the static first hyperpolarizability: from gas phase molecules to functionalized surfaces. *J Chem Phys*. 2013;138:204107. <https://doi.org/10.1063/1.4806259>
26. Praveen PA, Ramesh Babu R, Ramamurthi K. Theoretical and experimental investigations on linear and nonlinear optical response of metal complexes doped PMMA films. *Mater Res Express*. 2017;4:025024. <https://doi.org/10.1088/2053-1591/aa5cda>
27. Beaujean P, Champagne B, Grimme S, de Wergifosse M. All-atom quantum mechanical calculation of the second-harmonic generation of fluorescent proteins. *J Phys Chem Lett*. 2021;12:9684–90. <https://doi.org/10.1021/acs.jpclett.1c02911>
28. Lescos L, Beaujean P, Tonnelé C, Aurel P, Blanchard-Desce M, Rodriguez V, et al. Self-assembling, structure and nonlinear optical properties of fluorescent organic nanoparticles in water. *Phys Chem Chem Phys*. 2021;23:23643–54. <https://doi.org/10.1039/D1CP03741B>
29. Rossano-Tapia M, Brown A. Determination of two-photon-absorption cross sections using time-dependent density functional theory tight binding: application to fluorescent protein chromophores. *J Chem Theory Comput*. 2019;15:3153–61. <https://doi.org/10.1021/acs.jctc.9b00082>
30. Seibert J, Champagne B, Grimme S, de Wergifosse M. Dynamic structural effects on the second-harmonic generation of tryptophane-rich peptides and gramicidin A. *J Phys Chem B*. 2020;124:2568–78. <https://doi.org/10.1021/acs.jpcc.0c00643>
31. Chen K, Zheng X, Yang C, Tian WQ, Li W, Yang L. Theoretical studies on the electronic structure of nano-graphenes for applications in nonlinear optics. *Chem Res Chin Univ*. 2022;38:579–87. <https://doi.org/10.1007/s40242-021-1090-x>
32. Zheng X, Liu L, Yang C, He Y, Chen J, Tian WQ. Modulation of the second order nonlinear optical properties of helical graphene nanoribbons through introducing azulene defects or/and BN units. *Chem Res Chin Univ*. 2022;38:974–84. <https://doi.org/10.1007/s40242-021-1213-4>
33. Husch T, Vaucher AC, Reiher M. Semiempirical molecular orbital models based on the neglect of diatomic differential overlap approximation. *Int J Quant Chem*. 2018;118:e25799. <https://doi.org/10.1002/qua.25799>
34. Parr RG. A method for estimating electronic repulsion integrals over LCAO MO'S in complex unsaturated molecules. *J Chem Phys*. 1952;20:1499. <https://doi.org/10.1063/1.1700802>
35. Pople JA. Electron interaction in unsaturated hydrocarbons. *Trans Faraday Soc*. 1953;49:1375–85.
36. Christensen AS, Kubař T, Cui Q, Elstner M. Semiempirical quantum mechanical methods for noncovalent interactions for chemical and biochemical applications. *Chem Rev*. 2016;116:5301–37. <https://doi.org/10.1021/acs.chemrev.5b00584>
37. Ridley J, Zerner M. An intermediate neglect of differential overlap technique for spectroscopy: pyrrole and the azines. *Theor Chim Acta*. 1973;32:111–34. <https://doi.org/10.1007/BF00528484>
38. Dewar MJS, Thiel W. Ground states of molecules. 38. The MNDO method. Approximations and parameters. *J Am Chem Soc*. 1977;99:4899–907. <https://doi.org/10.1021/ja00457a004>
39. Dewar MJS, Zoebisch EG, Healy EF, Stewart JJP. Development and use of quantum mechanical molecular models. 76. AM1: a new general purpose quantum mechanical molecular model. *J Am Chem Soc*. 1985;107:3902–9. <https://doi.org/10.1021/ja00299a024>
40. Stewart JJP. Optimization of parameters for semiempirical methods I. Method *J Comput Chem*. 1989;10:209–20. <https://doi.org/10.1002/jcc.540100208>
41. Thiel W, Voityuk AA. Extension of the MNDO formalism to d orbitals: integral approximations and preliminary numerical results. *Theor Chim Acta*. 1992;81:391–404. <https://doi.org/10.1007/BF01134863>
42. Stewart JJP. Optimization of parameters for semiempirical methods V: modification of NDDO approximations and application to 70 elements. *J Mol Model*. 2007;13:1173–213. <https://doi.org/10.1007/s00894-007-0233-4>
43. Kolb M, Thiel W. Beyond the MNDO model: methodical considerations and numerical results. *J Comput Chem*. 1993;14:775–89. <https://doi.org/10.1002/jcc.540140704>
44. Thiel W. Semiempirical quantum-chemical methods. *WIREs Comput Mol Sci*. 2014;4:145–57. <https://doi.org/10.1002/wcms.1161>
45. Klopman G. A semiempirical treatment of molecular structures. II. Molecular terms and application to diatomic molecules. *J Am Chem Soc*. 1964;86:4550–7. <https://doi.org/10.1021/ja01075a008>
46. Bredow T, Jug K. Theory and range of modern semiempirical molecular orbital methods. *Theor Chem Acc*. 2005;113:1–14. <https://doi.org/10.1007/s00214-004-0610-3>
47. Hohenberg P, Kohn W. Inhomogeneous electron gas. *Phys Rev*. 1964;136:B864–71. <https://doi.org/10.1103/PhysRev.136.B864>
48. Kohn W, Sham LJ. Self-consistent equations including exchange and correlation effects. *Phys Rev*. 1965;140:A1133–8. <https://doi.org/10.1103/PhysRev.140.A1133>
49. Burke K, Ernzerhof M, Perdew JP. The adiabatic connection method: a non-empirical hybrid. *Chem Phys Lett*. 1997;265:115–20. [https://doi.org/10.1016/S0009-2614\(96\)01373-5](https://doi.org/10.1016/S0009-2614(96)01373-5)
50. Yang W. Generalized adiabatic connection in density functional theory. *J Chem Phys*. 1998;109:10107–10. <https://doi.org/10.1063/1.477701>
51. Yanai T, Tew DP, Handy NC. A new hybrid exchange–correlation functional using the coulomb-attenuating method (CAM-B3LYP). *Chem Phys Lett*. 2004;393:51–7. <https://doi.org/10.1016/j.cplett.2004.06.011>
52. Grimme S. Accurate description of van der Waals complexes by density functional theory including empirical corrections. *J Comput Chem*. 2004;25:1463–73. <https://doi.org/10.1002/jcc.20078>
53. Grimme S. Semiempirical GGA-type density functional constructed with a long-range dispersion correction. *J Comput Chem*. 2006;27:1787–99. <https://doi.org/10.1002/jcc.20495>
54. Grimme S, Antony J, Ehrlich S, Krieg H. A consistent and accurate ab initio parametrization of density functional dispersion correction (DFT-D) for the 94 elements H–Pu. *J Chem Phys*. 2010;132:154104. <https://doi.org/10.1063/1.3382344>



55. Caldeweyher E, Bannwarth C, Grimme S. Extension of the D3 dispersion coefficient model. *J Chem Phys*. 2017;147:034112. <https://doi.org/10.1063/1.4993215>
56. Seifert G. Tight-binding density functional theory: an approximate Kohn-Sham DFT scheme. *J Phys Chem A*. 2007;111:5609–13. <https://doi.org/10.1021/jp069056r>
57. Elstner M, Seifert G. Density functional tight binding. *Philos Trans R Soc A*. 2014;372:20120483. <https://doi.org/10.1098/rsta.2012.0483>
58. Seifert G, Eschrig H. LCAO- $X\alpha$  calculations of transition metal clusters. *Phys Status Solidi*. 1985;127:573–85. <https://doi.org/10.1002/pssb.2221270218>
59. Elstner M, Porezag D, Jungnickel G, Elsner J, Haugk M, Frauenheim T, et al. Self-consistent-charge density-functional tight-binding method for simulations of complex materials properties. *Phys Rev B*. 1998;58:7260–8. <https://doi.org/10.1103/PhysRevB.58.7260>
60. Gaus M, Cui Q, Elstner M. DFTB3: extension of the self-consistent-charge density-functional tight-binding method (SCC-DFTB). *J Chem Theory Comput*. 2011;7:931–48. <https://doi.org/10.1021/ct100684s>
61. Grimme S, Bannwarth C. Ultra-fast computation of electronic spectra for large systems by tight-binding based simplified Tamm-Dancoff approximation (sTDA-xTB). *J Chem Phys*. 2016;145:054103. <https://doi.org/10.1063/1.4959605>
62. Marenich AV, Jerome SV, Cramer CJ, Truhlar DG. Charge model 5: an extension of Hirshfeld population analysis for the accurate description of molecular interactions in gaseous and condensed phases. *J Chem Theory Comput*. 2012;8:527–41. <https://doi.org/10.1021/ct200866d>
63. Bannwarth C, Grimme S. sTDA-xTB for ground state calculations. 2016 <https://github.com/grimme-lab/xtb4stda>
64. Bannwarth C, Caldeweyher E, Ehlert S, Hansen A, Pracht P, Seibert J, et al. Extended tight-binding quantum chemistry methods. *WIREs Comput Mol Sci*. 2021;11:e1493.
65. Bannwarth C, Ehlert S, Grimme S. GFN2-xTB—an accurate and broadly parametrized self-consistent tight-binding quantum chemical method with multipole electrostatics and density-dependent dispersion contributions. *J Chem Theory Comput*. 2019;15:1652–71. <https://doi.org/10.1021/acs.jctc.8b01176>
66. Caldeweyher E, Ehlert S, Hansen A, Neugebauer H, Spicher S, Bannwarth C, et al. A generally applicable atomic-charge dependent London dispersion correction. *J Chem Phys*. 2019;150:154122. <https://doi.org/10.1063/1.5090222>
67. Bohle F, Grimme S. Efficient structural and energetic screening of fullerene encapsulation in a large supramolecular double decker macrocycle. *J Serb Chem Soc*. 2019;84:837–44.
68. Bursch M, Neugebauer H, Grimme S. Structure optimisation of large transition-metal complexes with extended tight-binding methods. *Angew Chem Int ed*. 2019;58:11078–87.
69. Neugebauer H, Bohle F, Bursch M, Hansen A, Grimme S. Benchmark study of electrochemical redox potentials calculated with semi-empirical and DFT methods. *J Phys Chem A*. 2020;124:7166–76.
70. Dohm S, Bursch M, Hansen A, Grimme S. Semiautomated transition state localization for organometallic complexes with semiempirical quantum chemical methods. *J Chem Theory Comput*. 2020;16:2002–12.
71. Schmitz S, Seibert J, Ostermeier K, Hansen A, Göller AH, Grimme S. Quantum chemical calculation of molecular and periodic peptide and protein structures. *J Phys Chem B*. 2020;124:3636–46. <https://doi.org/10.1021/acs.jpcc.0c00549>
72. Reis H. Problems in the comparison of theoretical and experimental hyperpolarizabilities revisited. *J Chem Phys*. 2006;125:014506. <https://doi.org/10.1063/1.2211611>
73. Olsen J, Jørgensen P. Linear and nonlinear response functions for an exact state and for an MCSCF state. *J Chem Phys*. 1985;82:3235–64.
74. Richardson LF, Gaunt JA. The deferred approach to the limit part I single lattice. Part II Interpenetrating lattices. *Philos Trans R Soc Lond A*. 1927;226:299–361.
75. Mohammed AAK, Limacher PA, Champagne B. Finding optimal finite field strengths allowing for a maximum of precision in the calculation of polarizabilities and hyperpolarizabilities. *J Comput Chem*. 2013;34:1497–507. <https://doi.org/10.1002/jcc.23285>
76. de Wergifosse M, Liégeois V, Champagne B. Evaluation of the molecular static and dynamic first hyperpolarizabilities. *Int J Quant Chem*. 2014;114:900–10. <https://doi.org/10.1002/qua.24685>
77. Ward JF. Calculation of nonlinear optical susceptibilities using diagrammatic perturbation theory. *Rev Mod Phys*. 1965;37:1–18. <https://doi.org/10.1103/RevModPhys.37.1>
78. Orr BJ, Ward JF. Perturbation theory of the non-linear optical polarization of an isolated system. *Mol Phys*. 1971;20:513–26. <https://doi.org/10.1080/00268977100100481>
79. Ullman A, Willand CS, Kohler W, Robello DR, Williams DJ, Handley L. New sulfonyl-containing materials for nonlinear optics: semi-empirical calculations, synthesis, and properties. *J Am Chem Soc*. 1990;112:7083–90. <https://doi.org/10.1021/ja00176a001>
80. Kanis DR, Ratner MA, Marks TJ. Calculation and electronic description of quadratic hyperpolarizabilities. Toward a molecular understanding of NLO responses in organotransition metal chromophores. *J Am Chem Soc*. 1992;114:10338–57. <https://doi.org/10.1021/ja00052a035>
81. Champagne B, Kirtman B. Evaluation of alternative sum-over-states expressions for the first hyperpolarizability of push-pull  $\pi$ -conjugated systems. *J Chem Phys*. 2006;125:024101. <https://doi.org/10.1063/1.2206181>
82. Sekino H, Bartlett RJ. Hyperpolarizabilities of the hydrogen fluoride molecule: a discrepancy between theory and experiment? *J Chem Phys*. 1986;84:2726–33. <https://doi.org/10.1063/1.450348>
83. Casida ME. Time-dependent density functional response theory for molecules. In: Chong DP, editor. Recent advances in density functional methods: (Part I). Singapore: World Scientific; 1995. p. 155–92.
84. von Neumann J, Wigner EP. Über das verhalten von eigenwerten bei adiabatischen prozessen. *Z Phys*. 1929;30:467.

85. von Neumann J, Wigner EP. Über das Verhalten von Eigenwerten bei adiabatischen Prozessen. In: Wightman AS, editor. The collected works of Eugene Paul Wigner. Part A: the scientific papers the collected works of Eugene Paul Wigner. Berlin, Heidelberg: Springer; 1993. p. 294. [https://doi.org/10.1007/978-3-662-02781-3\\_20](https://doi.org/10.1007/978-3-662-02781-3_20)
86. Kleinman DA. Nonlinear dielectric polarization in optical media. *Phys Rev.* 1962;126:1977–9.
87. Grimme S. A simplified Tamm-Dancoff density functional approach for the electronic excitation spectra of very large molecules. *J Chem Phys.* 2013;138:244104. <https://doi.org/10.1063/1.4811331>
88. Fetter AL, Walecka JD. Quantum theory of many-particle systems. New York: McGraw-Hill; 1971.
89. Bannwarth C, Grimme S. A simplified time-dependent density functional theory approach for electronic ultraviolet and circular dichroism spectra of very large molecules. *Comput Theor Chem.* 2014;1040-1041:45–53. <https://doi.org/10.1016/j.comptc.2014.02.023>
90. Löwdin P. On the non-orthogonality problem connected with the use of atomic wave functions in the theory of molecules and crystals. *J Chem Phys.* 1950;18:365–75. <https://doi.org/10.1063/1.1747632>
91. Ghosh DC, Islam N. Semiempirical evaluation of the global hardness of the atoms of 103 elements of the periodic table using the most probable radii as their size descriptors. *Int J Quant Chem.* 2010;110:1206–13. <https://doi.org/10.1002/qua.22202>
92. de Wergifosse M, Grimme S. Nonlinear-response properties in a simplified time-dependent density functional theory (sTD-DFT) framework: evaluation of the first hyperpolarizability. *J Chem Phys.* 2018;149:024108. <https://doi.org/10.1063/1.5037665>
93. de Wergifosse M, Seibert J, Grimme S. Simplified time-dependent density functional theory (sTD-DFT) for molecular optical rotation. *J Chem Phys.* 2020;153:084116. <https://doi.org/10.1063/5.0020543>
94. de Wergifosse M, Beaujean P, Grimme S. Ultrafast evaluation of two-photon absorption with simplified time-dependent density functional theory. *J Phys Chem A.* 2022;126:7534–47. <https://doi.org/10.1021/acs.jpca.2c02395>
95. Monson P, McClain W. Polarization dependence of the two-photon absorption of tumbling molecules with application to liquid 1-chloronaphthalene and benzene. *J Chem Phys.* 1970;53:29–37.
96. Wirth MJ, Koskela A, Sanders MJ. Molecular symmetry and two-photon spectroscopy. *Appl Spectrosc.* 1981;35:14–21.
97. Still WC, Tempczyk A, Hawley RC, Hendrickson T. Semianalytical treatment of solvation for molecular mechanics and dynamics. *J Am Chem Soc.* 1990;112:6127–9. <https://doi.org/10.1021/ja00172a038>
98. Cramer CJ, Truhlar DG. General parameterized SCF model for free energies of solvation in aqueous solution. *J Am Chem Soc.* 1991;113:8305–11. <https://doi.org/10.1021/ja00022a017>
99. Hawkins GD, Cramer CJ, Truhlar DG. Pairwise solute descreening of solute charges from a dielectric medium. *Chem Phys Lett.* 1995;246:122–9. [https://doi.org/10.1016/0009-2614\(95\)01082-K](https://doi.org/10.1016/0009-2614(95)01082-K)
100. Onsager L. Electric moments of molecules in liquids. *J Am Chem Soc.* 1936;58:1486–93. <https://doi.org/10.1021/ja01299a050>
101. Miertuš S, Scrocco E, Tomasi J. Electrostatic interaction of a solute with a continuum. A direct Utilizaion of AB initio molecular potentials for the prevision of solvent effects. *Chem Phys.* 1981;55:117–29. [https://doi.org/10.1016/0301-0104\(81\)85090-2](https://doi.org/10.1016/0301-0104(81)85090-2)
102. Miertues S, Tomasi J. Approximate evaluations of the electrostatic free energy and internal energy changes in solution processes. *Chem Phys.* 1982;65:239–45. [https://doi.org/10.1016/0301-0104\(82\)85072-6](https://doi.org/10.1016/0301-0104(82)85072-6)
103. Cammi R, Cossi M, Mennucci B, Tomasi J. Analytical Hartree–Fock calculation of the dynamical polarizabilities  $\alpha$ ,  $\beta$ , and  $\gamma$  of molecules in solution. *J Chem Phys.* 1996;105:10556–64. <https://doi.org/10.1063/1.472771>
104. Schweig A. Calculation of static electric higher polarizabilities of closed shell organic  $\pi$ -electron systems using a variation method. *Chem Phys Lett.* 1967;1:195–9. [https://doi.org/10.1016/0009-2614\(67\)85047-4](https://doi.org/10.1016/0009-2614(67)85047-4)
105. Oudar JL, Chemla DS. Hyperpolarizabilities of the nitroanilines and their relations to the excited state dipole moment. *J Chem Phys.* 1977;66:2664–8. <https://doi.org/10.1063/1.434213>
106. Matsuzawa N, Dixon DA. Semiempirical calculations of hyperpolarizabilities for extended  $\pi$  systems: polyenes, polyyenes, and polyphenyls. *Int J Quant Chem.* 1992;44:497–515. <https://doi.org/10.1002/qua.560440409>
107. Murphy DM, Mingos DMP, Haggitt JL, Marder TB. Synthesis of icosahedral carboranes for second-harmonic generation. Part 2t. *J Mater Chem.* 1993;3:3.
108. Beck B, Grummt UW. Semiempirical calculations of first-order hyperpolarizabilities: testing the performance of different methods in comparison to experiment. *J Phys Chem B.* 1998;102:664–70. <https://doi.org/10.1021/jp970592g>
109. Waite J, Papadopoulos MG. The effect of the H-bond interactions on the first hyperpolarisability of  $(\text{HF})_n$ . A comparative study. *Z Naturforsch A.* 1990;45:189–90. <https://doi.org/10.1515/zna-1990-0217>
110. Di Bella S, Fragala IL, Ratner MA, Marks TJ. Electron donor-acceptor complexes as potential high-efficiency second-order nonlinear optical materials. A computational investigation. *J Am Chem Soc.* 1993;115:682–6. <https://doi.org/10.1021/ja00055a043>
111. Castet F, Champagne B. Simple scheme to evaluate crystal nonlinear susceptibilities: semiempirical AM1 model investigation of 3-methyl-4-nitroaniline crystal. *J Phys Chem A.* 2001;105:1366–70. <https://doi.org/10.1021/jp003746s>
112. Zyss J. Hyperpolarizabilities of substituted conjugated molecules. I. Perturbed INDO approach to monosubstituted benzene. *J Chem Phys.* 1979;70:3333–40. <https://doi.org/10.1063/1.437918>
113. Zyss J. Hyperpolarizabilities of substituted conjugated molecules. II. Substituent effects and respective  $\sigma$ – $\pi$  contributions. *J Chem Phys.* 1979;70:3341–9. <https://doi.org/10.1063/1.437919>
114. Zyss J. Hyperpolarizabilities of substituted conjugated molecules. III. Study of a family of donor–acceptor disubstituted phenyl-polyenes. *J Chem Phys.* 1979;71:909–16. <https://doi.org/10.1063/1.438380>
115. Nalin de Silva KM. Semi empirical and ab initio methods for calculation of polarizability ( $\alpha$ ) and the hyperpolarizability ( $\beta$ ) of fluorenyl molecular system: a comparative investigation. *Comput Theor Chem.* 2005;725:243–6. <https://doi.org/10.1016/j.theochem.2005.02.067>

116. Yoshimura T. Enhancing second-order nonlinear optical properties by controlling the wave function in one-dimensional conjugated molecules. *Phys Rev B*. 1989;40:6292–8. <https://doi.org/10.1103/PhysRevB.40.6292>
117. Yoshimura T. Design and evaluation of organic nonlinear optical materials with a large Pockels effect. *Mol Cryst Liq Cryst*. 1990;182: 43–50. <https://doi.org/10.1080/00268949008047786>
118. Hammoutene D, Boucekkine G, Boucekkine A, Berthier G. The semiempirical challenge for the calculation of molecular hyperpolarizabilities. *Comput Theor Chem*. 1993;287:93–7. [https://doi.org/10.1016/0166-1280\(93\)87208-U](https://doi.org/10.1016/0166-1280(93)87208-U)
119. Barzoukas M, Fort A, Klein G, Boeglin A, Serbutoviez C, Oswald L, et al. Conformational dependence of the quadratic hyperpolarisabilities of a series of push-pull diaryl acetylenes: an experimental and computational investigation. *Chem Phys*. 1991;153:457–64. [https://doi.org/10.1016/0301-0104\(91\)80058-P](https://doi.org/10.1016/0301-0104(91)80058-P)
120. Zyss J, Berthier G. Nonlinear optical properties of organic crystals with hydrogen-bonded molecular units: the case of urea. *J Chem Phys*. 1982;77:3635–53. <https://doi.org/10.1063/1.444266>
121. Kurtz HA, Stewart JJP, Dieter KM. Calculation of the nonlinear optical properties of molecules. *J Comput Chem*. 1990;11:82–7. <https://doi.org/10.1002/jcc.540110110>
122. Nénon S, Champagne B. Origin of the surface-induced first hyperpolarizability in the C<sub>60</sub>/SiO<sub>2</sub> system: SCC-DFTB insight. *J Phys Chem Lett*. 2014;5:149–53. <https://doi.org/10.1021/jz402317x>
123. Cheng LT, Tam W, Marder SR, Stiegman AE, Rikken G, Spangler CW. Experimental investigations of organic molecular nonlinear optical polarizabilities. 2. A study of conjugation dependences. *J Phys Chem*. 1991;95:10643–52. <https://doi.org/10.1021/j100179a027>
124. Cheng LT, Tam W, Stevenson SH, Meredith GR, Rikken G, Marder SR. Experimental investigations of organic molecular nonlinear optical polarizabilities. 1. Methods and results on benzene and stilbene derivatives. *J Phys Chem*. 1991;95:10631–43. <https://doi.org/10.1021/j100179a026>
125. Di Bella S, Ratner MA, Marks TJ. Design of chromophoric molecular assemblies with large second-order optical nonlinearities. A theoretical analysis of the role of intermolecular interactions. *J Am Chem Soc*. 1992;114:5842–9. <https://doi.org/10.1021/ja00040a054>
126. Kanis DR, Ratner MA, Marks TJ, Zerner MC. Nonlinear optical characteristics of novel inorganic chromophores using the Zindo formalism. *Chem Mater*. 1991;3:19–22. <https://doi.org/10.1021/cm00013a009>
127. Barzoukas M, Blanchard-Desce M. Molecular engineering of push-pull dipolar and quadrupolar molecules for two-photon absorption: a multivalence-bond states approach. *J Chem Phys*. 2000;113:3951–9. <https://doi.org/10.1063/1.1288367>
128. He YY, Chen J, Zheng XL, Xu X, Li WQ, Yang L, et al. Spiral graphene nanoribbons with azulene defects as potential non-linear optical materials. *ACS Appl Nano Mater*. 2019;2:1648–54. <https://doi.org/10.1021/acsanm.9b00089>
129. Tian WQ. Modeling nonlinear optics of nanosystems with sum-over-states model. *J Comput Chem*. 2012;33:466–70. <https://doi.org/10.1002/jcc.21992>
130. Nicolaides CA, Papadopoulos M, Waite J. Calculations of induced moments in large molecules I. Polarizabilities and second hyperpolarizabilities in some alkanes. *Theor Chim Acta*. 1982;61:427–36. <https://doi.org/10.1007/BF00549035>
131. Papadopoulos MG, Waite J, Nicolaides CA. Calculations of induced moments in large molecules. II. Polarizabilities and second hyperpolarizabilities of some polyenes. *J Chem Phys*. 1982;77:2527–35. <https://doi.org/10.1063/1.444123>
132. Waite J, Papadopoulos MG, Nicolaides CA. Calculations of induced moments in large molecules. III. Polarizabilities and second hyperpolarizabilities of some aromatics. *J Chem Phys*. 1982;77:2536–9.
133. Waite J, Papadopoulos MG. Dependence of the polarizability,  $\alpha$ , and hyperpolarizabilities,  $\beta$  and  $\gamma$ , of a series of nitrogen heterocyclics on their molecular structure: a comparative study. *J Phys Chem*. 1990;94:1755–8. <https://doi.org/10.1021/j100368a010>
134. Mestechkin MM, Whyman GE. Time-dependent Hartree-Fock calculations of the quadratic polarizability dispersion for molecules with pronounced nonlinear optical properties. *Opt Commun*. 1993;95:92–6.
135. Parkinson WA, Zerner MC. The calculation of dynamic molecular polarizability. *J Chem Phys*. 1989;90:5606–11. <https://doi.org/10.1063/1.456413>
136. Abe J, Shirai Y. Heterocyclic betaines exhibiting extremely large first hyperpolarizability: ab initio and INDO/S calculations. *J Am Chem Soc*. 1996;118:4705–6. <https://doi.org/10.1021/ja9535017>
137. de Wergifosse M. Quantum chemical investigations of nonlinear optical compounds: from model to complex systems for second harmonic imaging microscopy. Namur, Belgium: Presse Universitaires de Namur (Université de Namur); 2014.
138. de Meulenaere E, Nguyen Bich N, de Wergifosse M, van Hecke K, van Meervelt L, Vanderleyden J, et al. Improving the second-order nonlinear optical response of fluorescent proteins: the symmetry argument. *J Am Chem Soc*. 2013;135:4061–9.
139. de Wergifosse M, Botek E, De Meulenaere E, Clays K, Champagne B. ONIOM investigation of the second-order nonlinear optical responses of fluorescent proteins. *J Phys Chem B*. 2018;122:4993–5005. <https://doi.org/10.1021/acs.jpcc.8b01430>
140. De Meulenaere E, Asselberghs I, de Wergifosse M, Botek E, Spaepen S, Champagne B, et al. Second-order nonlinear optical properties of fluorescent proteins for second-harmonic imaging. *J Mater Chem*. 2009;19:7514–9.
141. De Meulenaere E, de Wergifosse M, Botek E, Spaepen S, Champagne B, Vanderleyden J, et al. Nonlinear optical properties of mStrawberry and mCherry for second harmonic imaging. *J Nonlinear Opt Phys Mater*. 2010;19:1–13.
142. De Meulenaere E, de Wergifosse M, Botek E, Vanderleyden J, Champagne B, Clays K. Prediction of first hyperpolarizability of fluorescent proteins. *AIP Conference Proceedings*. 2015;1642:522–5.
143. Deniset-Besseau A, Duboiset J, Benichou E, Hache F, Brevet PF, Schanne-Klein MC. Measurement of the second-order hyperpolarizability of the collagen triple helix and determination of its physical origin. *J Phys Chem B*. 2009;113:13437–45.

144. de Wergifosse M, de Ruyck J, Champagne B. How the second-order nonlinear optical response of the collagen triple helix appears: a theoretical investigation. *J Phys Chem C*. 2014;118:8595–602.
145. Pracht P, Bohle F, Grimme S. Automated exploration of the low-energy chemical space with fast quantum chemical methods. *Phys Chem Chem Phys*. 2020;22:7169–92. <https://doi.org/10.1039/C9CP06869D>
146. Dubois J, Matar G, Besson F, Fichoux D, Benichou E, Russier-Antoine I, et al. Second harmonic generation from tryptophan-rich short peptides: WnKm and gramicidin a. *J Phys Chem B*. 2014;118:10413–8. <https://doi.org/10.1021/jp506416s>
147. de Coene Y, van Cleuvenbergen S, van Steerteghem N, Baekelandt V, Verbiest T, Bartic C, et al. Fluorescence-free spectral dispersion of the molecular first hyperpolarizability of bacteriorhodopsin. *J Phys Chem C*. 2017;121:6909–15. <https://doi.org/10.1021/acs.jpcc.7b00625>
148. Evleth EM, Peticolas WL. Two-photon capture cross sections of pyrene and Benzpyrene from SCF–MO calculations. *J Chem Phys*. 1964;41:1400–7. <https://doi.org/10.1063/1.1726080>
149. Pariser R, Parr RG. A semi-empirical theory of the electronic spectra and electronic structure of complex unsaturated molecules. *J Chem Phys*. 1953;21:466–71.
150. Honig B, Jortner J, Szöke A. Theoretical studies of two-photon absorption processes. I Molecular benzene. *J Chem Phys*. 1967;46:2714–27.
151. Twarowski A, Klinger D. A search for a low-lying excited  $1a$  state in 1, 3, 5-hexatriene. *Chem Phys Lett*. 1977;50:36–40. [https://doi.org/10.1016/0009-2614\(77\)80675-1](https://doi.org/10.1016/0009-2614(77)80675-1)
152. Birge RR, Pierce BM. A theoretical analysis of the two-photon properties of linear polyenes and the visual chromophores. *J Chem Phys*. 1979;70:165–78.
153. Birge RR, Bennett JA, Pierce BM, Thomas TM. Two-photon spectroscopy of the visual chromophores. Evidence for a lowest excited  $^1A_g$ -like  $\pi\pi^*$  state in *all-trans*-retinol (vitamin A). *J Am Chem Soc*. 1978;100:1533–9.
154. Marchese FT, Seliskar C, Jaffé H. The use of CNDO in spectroscopy. XV. Two photon absorption. *J Chem Phys*. 1979;72:4194–203.
155. Albota M, Beljonne D, Brédas JL, Ehrlich JE, Fu JY, Heikal AA, et al. Design of organic molecules with large two-photon absorption cross sections. *Science*. 1998;281:1653–6. <https://doi.org/10.1126/science.281.5383.1653>
156. Zheng S, Leclercq A, Fu J, Beverina L, Padilha LA, Zojer E, et al. Two-photon absorption in quadrupolar bis (acceptor)-terminated chromophores with electron-rich bis (heterocycle) vinylene bridges. *Chem Mater*. 2007;19:432–42.
157. Masunov A, Tretiak S. Prediction of two-photon absorption properties for organic chromophores using time-dependent density-functional theory. *J Phys Chem B*. 2004;108:899–907.
158. Frediani L, Rinkevicius Z, Ågren H. Two-photon absorption in solution by means of time-dependent density-functional theory and the polarizable continuum model. *J Chem Phys*. 2005;122:244104.
159. Day PN, Nguyen KA, Pachter R. Calculation of two-photon absorption spectra of donor- $\pi$ -acceptor compounds in solution using quadratic response time-dependent density functional theory. *J Chem Phys*. 2006;125:094103.
160. Terenzi F, Katan C, Badaeva E, Tretiak S, Blanchard-Desce M. Enhanced two-photon absorption of organic chromophores: theoretical and experimental assessments. *Adv Mater*. 2008;20:4641–78.
161. Day PN, Nguyen KA, Pachter R. Calculation of one-photon and two-photon absorption spectra of porphyrins using time-dependent density functional theory. *J Chem Theory Comput*. 2008;4:1094–106.
162. Hrobáriková V, Hrobárik P, Gajdoš P, Ftilis I, Fakis M, Persephonis P, et al. Benzothiazole-based fluorophores of donor- $\pi$ -acceptor- $\pi$ -donor type displaying high two-photon absorption. *J Phys Org Chem*. 2010;75:3053–68.
163. Day PN, Nguyen KA, Pachter R. Calculation of one- and two-photon absorption spectra of thiolated gold nanoclusters using time-dependent density functional theory. *J Chem Theory Comput*. 2010;6:2809–21.
164. Vivas MG, Silva DL, Misoguti L, Zalesny R, Bartkowiak W, Mendonca CR. Degenerate two-photon absorption in *all-trans* retinal: nonlinear spectrum and theoretical calculations. *J Phys Chem A*. 2010;114:3466–70.
165. De Boni L, Correa DS, Silva DL, Gonçalves PJ, Zilio SC, Parra GG, et al. Experimental and theoretical study of two-photon absorption in nitrofur derivatives: promising compounds for photochemotherapy. *J Chem Phys*. 2011;134:014509.
166. Ohta K, Yamada S, Kamada K, Slepov AD, Hegmann FA, Tykwinski RR, et al. Two-photon absorption properties of two-dimensional  $\pi$ -conjugated chromophores: combined experimental and theoretical study. *J Phys Chem A*. 2011;115:105–17.
167. Palczewska G, Vinberg F, Stremplewski P, Bircher MP, Salom D, Komar K, et al. Human infrared vision is triggered by two-photon chromophore isomerization. *Proc Natl Acad Sci U S A*. 2014;111:E5445–54.
168. Bednarska J, Zalesny R, Tian G, Murugan NA, Ågren H, Bartkowiak W. Nonempirical simulations of inhomogeneous broadening of electronic transitions in solution: predicting band shapes in one- and two-photon absorption spectra of chalcones. *Molecules*. 2017;22:1643.
169. Di Remigio R, Giovannini T, Ambrosetti M, Cappelli C, Frediani L. Fully polarizable QM/fluctuating charge approach to two-photon absorption of aqueous solutions. *J Chem Theory Comput*. 2019;15:4056–68.
170. Yu D, Hu Y, Zhang G, Li W, Jiang Y. Theoretical studies on the two-photon absorption of II–VI semiconductor nanoclusters. *Sci Rep*. 2022;12:110.
171. Snedkov K, Olsen JMH, Schwabe T, Hättig C, Christiansen O, Kongsted J. Computational screening of one- and two-photon spectrally tuned channel rhodopsin mutants. *Phys Chem Chem Phys*. 2013;15:7567–76.
172. List NH, Pimenta FM, Holmegaard L, Jensen RL, Etzerodt M, Schwabe T, et al. Effect of chromophore encapsulation on linear and nonlinear optical properties: the case of “miniSOG,” a protein-encased flavin. *Phys Chem Chem Phys*. 2014;16:9950–9.



173. Beerepoot MTP, Friese DH, Ruud K. Intermolecular charge transfer enhances two-photon absorption in yellow fluorescent protein. *Phys Chem Chem Phys*. 2014;16:5958–64.
174. Beerepoot MT, Friese DH, List NH, Kongsted J, Ruud K. Benchmarking two-photon absorption cross sections: performance of CC2 and CAM-B3LYP. *Phys Chem Chem Phys*. 2015;17:19306–14.
175. Beerepoot MTP, Alam MM, Bednarska J, Bartkowiak W, Ruud K, Zalesny R. Benchmarking the performance of exchange correlation functionals for predicting two-photon absorption strengths. *J Chem Theory Comput*. 2018;14:3677–85.
176. Grabarek D, Andruniów T. Assessment of functionals for TDDFT calculations of one- and two-photon absorption properties of neutral and anionic fluorescent proteins chromophores. *J Chem Theory Comput*. 2019;15:490–508.
177. Zalesny R, Alam MM, Day PN, Nguyen KA, Pachter R, Lim CK, et al. Computational design of two-photon active organic molecules for infrared responsive materials. *J Mater Chem C*. 2020;8:9867–73.
178. Nayyar IH, Masunov AE. Two-photon absorption spectra predicted by semiempirical methods. *J Comput Theor Nanosci*. 2014;11:2208–20.
179. Drobizhev M, Makarov NS, Tillo SE, Hughes TE, Rebane A. Two-photon absorption properties of fluorescent proteins. *Nat Methods*. 2011;8:393–9.
180. Katan C, Tretiak S, Werts MH, Bain AJ, Marsh RJ, Leonczek N, et al. Two-photon transitions in quadrupolar and branched chromophores: experiment and theory. *J Phys Chem B*. 2007;111:9468–83.
181. Homans RJ, Khan RU, Andrews MB, Kjeldsen AE, Natrajan LS, Marsden S, et al. Two photon spectroscopy and microscopy of the fluorescent flavoprotein, iLOV. *Phys Chem Chem Phys*. 2018;20:16949–55.
182. Cronstrand P, Christiansen O, Norman P, Ågren H. Theoretical calculations of excited state absorption. *Phys Chem Chem Phys*. 2000;2:5357–63. <https://doi.org/10.1039/b006782m>
183. Mikhailov IA, Tafur S, Masunov AE. Double excitations and state-to-state transition dipoles in  $\pi$ - $\pi^*$  excited singlet states of linear polyenes: time-dependent density-functional theory versus multiconfigurational methods. *Phys Rev A*. 2008;77:012510. <https://doi.org/10.1103/PhysRevA.77.012510>
184. Avagliano D, Bonfanti M, Nenov A, Garavelli M. Automatized protocol and Interface to simulate QM/MM time-resolved transient absorption at TD-DFT level with COBRAMM. *J Comput Chem*. 2022;43:1641–55. <https://doi.org/10.1002/jcc.26966>
185. Fischer SA, Cramer CJ, Govind N. Excited-state absorption from real-time time-dependent density functional theory: optical limiting in zinc phthalocyanine. *J Phys Chem Lett*. 2016;7:1387–91. <https://doi.org/10.1021/acs.jpclett.6b00282>
186. Radziuk D, Möhwald H. Ultrasonically treated liquid interfaces for progress in cleaning and separation processes. *Phys Chem Chem Phys*. 2016;18:21–46. <https://doi.org/10.1039/C5CP05142H>
187. Fedotov DA, Paul AC, Koch H, Santoro F, Coriani S, Improta R. Excited state absorption of DNA bases in the gas phase and in chloroform solution: a comparative quantum mechanical study. *Phys Chem Chem Phys*. 2022;24:4987–5000. <https://doi.org/10.1039/D1CP04340D>
188. Kanis DR, Lacroix PG, Ratner MA, Marks TJ. Electronic structure and quadratic hyperpolarizabilities in organotransition-metal chromophores having weakly coupled  $\pi$ -networks. Unusual mechanisms for second-order response. *J Am Chem Soc*. 1994;116:10089–102. <https://doi.org/10.1021/ja00101a030>
189. Muñoz-Losa A, Curutchet C, Galván IF, Mennucci B. Quantum mechanical methods applied to excitation energy transfer: a comparative analysis on excitation energies and electronic couplings. *J Chem Phys*. 2008;129:034104. <https://doi.org/10.1063/1.2953716>
190. Sun M, Chen J, Xu H. Visualizations of transition dipoles, charge transfer, and electron-hole coherence on electronic state transitions between excited states for two-photon absorption. *J Chem Phys*. 2008;128:064106. <https://doi.org/10.1063/1.2829407>
191. Deshayé MY, Wrede AT, Kowalczyk T. Electronic transition dipole moments from time-independent excited-state density-functional tight-binding. *J Chem Phys*. 2023;158:134104. <https://doi.org/10.1063/5.0139023>
192. Guldi DM, Prato M. Excited-state properties of C60 fullerene derivatives. *Acc Chem Res*. 2000;33:695–703. <https://doi.org/10.1021/ar990144m>
193. Seibert J, Bannwarth C, Grimme S. Biomolecular structure information from high-speed quantum mechanical electronic spectra calculation. *J Am Chem Soc*. 2017;139:11682–5.
194. Changelnet-Barret P, Plaza P, Martin MM, Chosrowjan H, Taniguchi S, Mataga N, et al. Role of arginine 52 on the primary photoinduced events in the PYP photocycle. *Chem Phys Lett*. 2007;434:320–5.
195. Grummt UW, Lehmann F, Rentsch S, Hein J, Helbig M. Second order hyperpolarizability of hydroxystilbazolium salts and their betaines-relationship to chemical structure. *J Mater Chem*. 1999;9:1419–24.
196. Zheng XL, Yang L, Shang B, Wang MQ, Niu Y, Li WQ, et al. Two-dimensional two-photon absorptions and third-order nonlinear optical properties of Ih fullerenes and fullerene anions. *Phys Chem Chem Phys*. 2020;22:14225–35. <https://doi.org/10.1039/D0CP01996H>
197. Malagoli M, Thiel W. A semiempirical approach to nonlinear optical properties of large molecules at the MNDO and MNDOD level. *Chem Phys*. 1996;206:73–85. [https://doi.org/10.1016/0301-0104\(96\)00011-0](https://doi.org/10.1016/0301-0104(96)00011-0)
198. Avcı D. The consistency analysis of different semiempirical calculations on second- and third-order nonlinear optical properties of donor-acceptor chromophores containing  $\alpha$ -cyan. *Spectrochim Acta A*. 2010;77:665–72. <https://doi.org/10.1016/j.saa.2010.07.007>
199. Avcı D. Second and third-order nonlinear optical properties and molecular parameters of azo chromophores: semiempirical analysis. *Spectrochim Acta A*. 2011;82:37–43. <https://doi.org/10.1016/j.saa.2011.06.037>
200. Bishop DM, Gu FL. Ab initio and semi-empirical studies of the static polarizability and the second hyperpolarizability of diamond: finite td symmetry models from CH<sub>4</sub> to C<sub>281</sub>H<sub>172</sub>. *Chem Phys Lett*. 2000;317:322–9. [https://doi.org/10.1016/S0009-2614\(99\)01337-8](https://doi.org/10.1016/S0009-2614(99)01337-8)

201. van Steerteghem N, Clays K, Verbiest T, van Cleuvenbergen S. Third-harmonic scattering for fast and sensitive screening of the second hyperpolarizability in solution. *Anal Chem*. 2017;89:2964–71. <https://doi.org/10.1021/acs.analchem.6b04429>
202. Rodriguez V. Polarization-resolved third-harmonic scattering in liquids. *J Phys Chem C*. 2017;121:8510–4. <https://doi.org/10.1021/acs.jpcc.7b00983>
203. de Wergifosse M, Bannwarth C, Grimme S. A simplified spin-Flip time-dependent density functional theory approach for the electronic excitation spectra of very large diradicals. *J Phys Chem A*. 2019;123(27):5815–25. <https://doi.org/10.1021/acs.jpca.9b03176>
204. Grimme S, Neese F. Double-hybrid density functional theory for excited electronic states of molecules. *J Chem Phys*. 2007;127(15):154116. <https://doi.org/10.1063/1.2772854>
205. Goerigk L, Moellmann J, Grimme S. Computation of accurate excitation energies for large organic molecules with double-hybrid density functionals. *Phys Chem Chem Phys*. 2009;11(22):4611–20. <https://doi.org/10.1039/b902315a>
206. Zhang X, Herbert JM. Spin-flip, tensor equation-of-motion configuration interaction with a density-functional correction: a spin-complete method for exploring excited-state potential energy surfaces. *J Chem Phys*. 2015;143(23):234107. <https://doi.org/10.1063/1.4937571>
207. Lee S, Filatov M, Lee S, Choi CH. Eliminating spin-contamination of spin-flip time dependent density functional theory within linear response formalism by the use of zeroth-order mixed-reference (MR) reduced density matrix. *J Chem Phys*. 2018;149(10):104101. <https://doi.org/10.1063/1.5044202>
208. Niehaus TA, Suhai S, Della Sala F, Lugli P, Elstner M, Seifert G, et al. Tight-binding approach to time-dependent density-functional response theory. *Phys Rev B*. 2001;63:085108.
209. Norman P, Bishop DM, Jensen HJA, Oddershede J. Near-resonant absorption in the time-dependent self-consistent field and multi-configurational self-consistent field approximations. *J Chem Phys*. 2001;115:10323–34. <https://doi.org/10.1063/1.1415081>
210. Norman P, Bishop DM, Jensen HJA, Oddershede J. Nonlinear response theory with relaxation: the first-order hyperpolarizability. *J Chem Phys*. 2005;123:194103. <https://doi.org/10.1063/1.2107627>
211. Kristensen K, Kauczor J, Kjrgaard T, Jørgensen P. Quasienergy formulation of damped response theory. *J Chem Phys*. 2009;131:044112. <https://doi.org/10.1063/1.3173828>
212. Rodriguez V, Verreault D, Adamietz F, Kalafatis A. All-optical measurements of the Verdet constant in achiral and chiral liquids: toward all-optical magnetic spectroscopies. *ACS Photon*. 2022;9:2510–9. <https://doi.org/10.1021/acsphotonics.2c00720>
213. Bonvicini A, Forbes KA, Andrews DL, Champagne B. Hyper-Rayleigh scattering optical activity: theory, symmetry considerations, and quantum chemistry applications. *J Chem Phys*. 2023;158:204103. <https://doi.org/10.1063/5.0152784>

**How to cite this article:** Löffelsender S, Beaujean P, de Wergifosse M. Simplified quantum chemistry methods to evaluate non-linear optical properties of large systems. *WIREs Comput Mol Sci*. 2023. e1695. <https://doi.org/10.1002/wcms.1695>